11-2018

Quantification of Cloud Condensation Nuclei Effects on the Microphysical Structure of Continental Thunderstorms Using Polarimetric Radar Observations

Kun-Yuan Lee
University of Nebraska-Lincoln, jasonklee@huskers.unl.edu

QUANTIFICATION OF CLOUD CONDENSATION NUCLEI EFFECTS ON THE MICROPHYSICAL STRUCTURE OF CONTINENTAL THUNDERSTORMS USING POLARIMETRIC RADAR OBSERVATIONS

by

Kun-Yuan Lee

A THESIS

Presented to the Faculty of

The Graduate College at the University of Nebraska

In Partial Fulfillment of Requirements

For the Degree of Master of Science

Major: Earth and Atmospheric Sciences

Under the Supervision of Professor Matthew S. Van Den Broeke

Lincoln, Nebraska

November, 2018

QUANTIFICATION OF CLOUD CONDENSATION NUCLEI EFFECTS ON THE MICROPHYSICAL STRUCTURE OF CONTINENTAL THUNDERSTORMS USING POLARIMETRIC RADAR OBSERVATIONS

Kun-Yuan Lee, M.S.

University of Nebraska, 2019

Advisor: Matthew S. Van Den Broeke

Aerosols serving as cloud condensation nuclei (CCN) are crucial to the microphysical structure of thunderstorms. They can also alter the rate of cloud microphysical processes, the moisture profile and the local temperature as a result of latent heating/cooling in the early stage of thunderstorm development. Continental thunderstorms are characterized by high complexity and are highly influenced by environmental conditions. The purpose of this study is to determine the influences of CCN concentration on the microphysics of continental thunderstorms, using a sample of storms from northwestern Oklahoma. The Weather Surveillance Radar-1988 Doppler (WSR-88D) at Vance Air Force Base (KVNX) was upgraded to dual-polarimetric capabilities in March 2011. Using polarimetric variables, a technique using ArcGIS (Geographic Information System) is used to identify the mean droplet characteristics. An estimate of the mean droplet size from the freezing level to 0.5 km above and the warm updraft depth above the ambient freezing level is developed for 36 continental thunderstorms within 15-20 minutes of convection initiation. Data from the Atmospheric

Radiation Measurement (ARM) program at the Southern Great Plains (SGP) site are used to represent the aerosol concentration of the thunderstorm environment, and model soundings from the Rapid Update Cycle (RUC) and Rapid Refresh (RAP) Model are used to describe the storm environment. The RUC/RAP soundings were located approximate 59 km away from KVNX and were selected to represent the undisturbed far-field environment. Previous observational and modeling studies found effects of CCN concentration on thunderstorm characteristics including stronger updrafts as a result of enhanced latent heating, suppressed rain drop collision and coalescence, and altering the cold pool size. The results of this study provide more substantial observational evidence in support of these prior findings.

Dedication

I dedicate all my appreciation to my family and friends who provide endless support and unconditional love,

and also to

the memory of

my grandfather Ching-Chia Lee.

Acknowledgments

First and foremost, I would like to thank my advisor, Dr. Matthew S. Van Den Broeke, who provided me with the research opportunity in the past one and half years of graduate study. His patience and guidance reinforce my imagination, creativity, and passion in atmospheric science during my undergraduate and continues through my graduate careers. He also led me through the never-ending challenge presented by the fluidity of the natural world. I would also like to thank my committee members, Dr. Clinton Rowe and Dr. Adam Houston for their insightful knowledge and professional suggestion as I went through the research process. This work would not have been possible without the financial support from National Science Foundation (AGS-1748012) and the Department of Earth and Atmospheric Science at the University of Nebraska-Lincoln for providing me a friendly environment to complete this project. I would also like to give a special thanks to my graduate school colleagues and officemates, Matthew Wilson, Nancy Barnhardt, and Graupel for their expertise, knowledge, encouragements, humor, and patience along this journey.

Table of Contents

List of Figures

List of Tables

1. Introduction

Some aerosols may serve as CCN and have a substantial effect on cloud microphysics, especially during the early stage of thunderstorm development. In an environment with a high aerosol concentration, thunderstorms tend to suppress coalescence due to smaller drop size and narrower drop size distribution, causing raindrops to ascend to a higher level and resulting in more supercooled water droplets and accretion on ice particles compared to relatively aerosol-free thunderstorms. This effect is more significant in warm-based clouds (cloud base ≥ 20°C) and less significant in cold-based clouds (cloud base ≤ 20°C) (Rosenfeld and Bell 2011).

Previous studies (e.g., Bell et al. 2008; Rosenfeld and Bell 2011) point to a positive relationship between cloud formation in an aerosol-rich environment and storm invigoration. Work by May et al. (2011) using polarimetric radar observations indicated that a high-aerosol environment results in a lower concentration of large drops at the lower levels of a storm. Simulations performed with a higher aerosol concentration indicate a reduction of the warm and cold rain processes in supercells reducing the precipitation rate within the forward and rear-flank downdrafts as aerosol alters the local temperature and moisture profiles. It slows the evaporative cooling rate and produces a weaker cool pool that allows vertical stacking of low-level vorticity and the storm-scale mesocyclone along the rear-flank downdraft (Lerach et al. 2008). An aerosol-induced change of the precipitation distribution may also alter the magnitude of evaporative cooling in the precipitation shaft, altering the possibility and/or magnitude of severe weather events. Three-dimensional simulations conducted by Lerach and Cotton (2012) found CCN microphysical effects on supercell storms' near-surface environments and

precipitation rate. This indirect effect may modify the cold-pool intensity, affecting the likelihood of tornadogenesis (Lerach et al. 2008).

Much research indicates that aerosol concentration alters the microphysical structure of thunderstorms during their early stage and may have a substantial impact later in the events. (e.g., Andreae et al. 2004; Koren et al. 2005; Fan et al. 2007). Simulation by (Ilotoviz et al. 2018) found the height and volume of Z_{DR} columns varied according to the aerosol concentration, and the aerosol effects on simulated supercell thunderstorms were examined by Kalina et al. (2014). However, few observational studies contain quantification of aerosol concentration effects using polarimetric radar measurements (e.g., May et al. 2011), and no studies have examined these effects in continental thunderstorms in the central United States, a region with frequent active convection during the summer. This region is also influenced by wildfires from Central America during the late spring and early summer (Wang et al. 2009). Hence, this study seeks to provide preliminary observational results quantifying CCN effects on the microphysical structure of continental thunderstorms during the warm season (May to August) using polarimetric radar and RUC/RAP soundings to control for local environmental variability. Given the large natural variability in the evolution of DSDs, mean differential reflectivity (Z_{DR}) of individual storms in their early growth stage will be presented. Effects of CCN concentration on updraft characteristics will also be examined since it is hypothesized that large CCN concentration should lead to updraft invigoration.

2. Background

I. Continental Thunderstorms

Continental thunderstorms are convective storms which initiate inland, or the airmass spends 12 or more hours over land prior to convection initiation (Wilson et al. 2011). They can become intense over certain areas if the environment is correct, including one of the most active regions: the south-central United States (Zipser et al. 2006), which is the primary research area for this study. Continental thunderstorms may be accompanied by heavy rain, strong wind, and hail. They can often be very complex, with different convective modes depending on environmental conditions including instability. Continental thunderstorms are a staple feature of the summer climate across the central and eastern United States and are usually fueled by diurnal instability, often forming daily in the afternoon in hot, moist air masses of the southern U.S. (Miller and Mote 2017). Continental thunderstorms can become supercellular if the environmental conditions are correct (e.g., the correct ratio of shear to instability is present). These supercells contain a long-lived mesocyclone and are most common in the central United States (Thompson 1998). They have the potential to be more severe than other types of thunderstorms. Supercells typically exhibit known radar signatures including a bounded weak echo region (BWER), differential reflectivity (Z_{DR}) column, Z_{DR} arc and hook echo.

II. Dual-Polarimetric Radar

The implementation of polarimetric radar to the NWS (National Weather Service) network was completed in 2013. In addition to the conventional radar using single polarization to measure the radar reflectivity factor (Z_{HH}), Doppler velocity, and spectrum

width, a polarimetric radar also measures the vertical reflectivity factor (Z_{VV}) (e.g., Kumjian 2013). Other, derived variables include Z_{DR}, specific differential phase (K_{DP}) and the copolar cross-correlation coefficient (ρ_{HV}). These variables can be used to obtain additional information such as the size, shape, and orientation of targets within a radar sample volume (e.g., Kumjian 2013).

The radar reflectivity factor (Z_{HH}) varies depending on particle size, phase, and composition. Larger particle sizes are associated with higher reflectivity as more backscattered radiation returns to the radar. This variable is defined as:

$$P_e = kP_s \cdot \left(\frac{\varepsilon}{\lambda^4 \cdot R^2}\right) \sum ND^6, \quad Z_{HH} = \int_0^\infty N(D)D^6 dD \qquad (1)$$

Where k is dielectric constant factor; P_s denotes the transmitted power (watts), and λ is the radar transmitted wavelength (cm); ε represents the dielectric constant (ice or liquid drops), N is the number of scatterers in the sample volume and D is the equivalent diameter (cm) of scatterers within a unit volume within the beam (Wolff 2018).

When determining the Z_{HH} value, the difference in dielectric constant between liquid and ice scatterers should be considered; it represents the ability of a substance to store energy in an electric field. For example, ice particles have smaller dielectric constant (can be as low as 0.208) than liquid droplets (~0.93 for water at 310 K; e.g., Lunkenheimer et al. 2017). Hence, it is essential to consider the droplet sizes and phase difference (liquid, ice and mixed) especially when measuring above the environmental freezing level, as often supercooled water droplets and ice crystals may coexist as the cloud becomes mixed-phase (Rosenfeld et al. 2000). Moreover, the radar reflectivity may also vary as a function of DSD since reflectivity is proportional to drop diameter to the sixth power.

Differential reflectivity (Z_{DR}) in units of decibels (dB) provides a measure of scatterer orientation and is the ratio of the reflectivity between horizontal polarization and vertical polarization (Doviak and Zrnić, 2006). It can be used to characterize the median diameter (D_0) of the drop size distribution (Seliga and Bringi 1976). Positive values indicate that the targets are larger in the horizontal dimension than the vertical dimension. It can provide an estimate of aspects of the raindrop size distribution and infer regions of liquid water and mixed-phase hydrometeors in combination with other variables. Aggregated ice crystals typically have a Z_{DR} value less than or equal to zero. Columns and plates can have positive values ranging from 2 to 4 dB (Kumjian and Ryzhkov 2007). The Z_{DR} is also lower in ice particles with the same shape and orientation as raindrops, as the dielectric constant is much lower for ice. A decrease in Z_{DR} coincident increase in Z_{HH} is often associated with large hailstones (e.g., Kumjian and Ryzhkov 2008).

Copolar cross-correlation coefficient (hereafter correlation coefficient) is a measure of the correlation between the returned power signals from the horizontally and vertically polarized pulses. It is also a good indicator of echoes of meteorological significance as such hail and ice (WDTD 2013). Correlation coefficient typically decreases with range since the sample volume has broadened and included a greater diversity of hydrometeor species. Correlation coefficient can also be reduced by a mixture of scatterer sizes or the inclusion of any hailstones or non-meteorological scatter (e.g., birds or insects; Van Den Broeke 2013). It is also useful to determine the uniformity of raindrop characteristics within a given sample volume.

III. Differential Reflectivity Columns

A polarimetric signature associated with thunderstorm updrafts, the Z_{DR} column, has been widely studied in the literature (e.g., Conway and Zrnić 1993; Kumjian and Ryzhkov 2008; Snyder et al. 2013; Kumjian et al. 2014; Plummer et al. 2018). The height of the Z_{DR} column is typically defined as the distance between the environmental freezing level and the highest altitude with a Z_{DR} value of at least 1 dB (Figure 2.1; e.g., Kumjian 2014; Snyder et al. 2015; Van Den Broeke 2016). The column can extend up to a few kilometers beyond the environmental freezing level, with $Z_{DR} > 3$ dB indicating the presence of large, oblate hydrometers or water-coated hailstones (Kumjian and Ryzhkov 2008). Prior studies (e.g., Alberoni et al. 2000) discovered that the Z_{DR} column is consistently found on the inflow side of a storm or fringe of the updraft, and it also can be found within or on the periphery of a weak echo region if the storm updraft is strong enough. Deepening of the column in convective cells may indicate the updraft is intensifying and may be used as a diagnosis of storm intensification. Kumjian (2014) found the height of the Z_{DR} column is correlated with an increase in Z_{HH} above the freezing level. In Hubbert et al. (1998), the temporal evolution of Z_{DR} included a positive correlation between the column and the center of an intensifying updraft. Hubbert et al. (1998) also found Z_{DR} column across low-level inflow will result in a less-broad DSD at the lower level the storm due to sorting. Ilotoviz et al. (2018) found the height and volume of Z_{DR} columns increase with an increase in aerosol concentration (Figure 2.2), and that characteristics of Z_{DR} columns are highly correlated with vertical velocity, hail size, and aerosol concentration. In addition, simulations performed by Ilotoviz et al. (2018) found the height of the Z_{DR} column is substantially larger in the case of high aerosol concentration, and the height of the 1 dB contour in polluted cases (defined as

aerosol concentration >3000 cm^{-3}) is higher than in clean cases (defined as <100 cm^{-3}) by about 1 km (Figure 2.3). The numerical study of Ilotoviz et al. (2018) found lower CCN cases generally had smaller Z_{DR} columns but also weaker updrafts, and cases with higher CCN had larger Z_{DR} columns and stronger updrafts. This indicates that the Z_{DR} column could be used for evaluating the vertical velocity in a deep convective cloud.

IV. Aerosols Affect Storm Microphysics Leading to Storm Invigoration

Atmospheric aerosols, produced by both anthropogenic activities and natural processes, serve as cloud condensation nuclei (CCN) and are crucial to the microphysical structure of thunderstorms. Condensation nuclei (CN) described by Tao et al. (2012) are aerosol particles composed of hygroscopic materials which provide a platform for water vapor to condense. In general, the aerosol-rich region has more CN. However, not all CN can effectively serve as CCN. In order for CN to serve as CCN, the ambient saturation ratio must exceed a critical saturation ratio (activation saturation ratio), which is a function of supersaturation corresponding to given particle species. The CCN spectrum is followed using Pruppacher and Klett (1997) as below:

$$N_{\mathrm{CCN}} = CS^{K} \tag{2}$$

where N_{CCN} is the number concentration of activated cloud condensation [cm^{-3}], S is the supersaturation ratio (%), C is the CCN concentration at S = 1%, and K is a dimensionless constant.

Many past studies have hypothesized that when more aerosol particles are advected into a thunderstorm, CCN concentration is also increased at the lower level of the storm, and raindrops are more numerous compared to a relatively clean environment. CCN include

the proportion of CN that behaves differently depending on the supersaturation value and strongly depends on the mass, composition of their water-soluble component and the ambient conditions. The equilibrium saturation ratio over the solution drop surface was first introduced by Köhler (1936), which is commonly described as Köhler's curve with larger aerosols having the advantage of easier activation (Tao et al. 2012). CN are also influenced by aerosol source patterns (e.g., urban pollution and biomass burning; Burkart et al. 2011). A clean environment has fewer CCN, thus fewer raindrops form in an equivalent updraft volume leading to less competition for water vapor and therefore larger droplets. In addition, depending on the aerosol concentration and environment conditions, the aerosol-induced formation of more raindrops and total liquid water content can lead to greater latent heat release in the storm updraft, creating a deeper and stronger updraft and higher potential for increased hail size and precipitation rate than in the case of high CCN concentration.

The influence of aerosols on convective storms include two major components: direct and indirect. Direct effect are resulted of aerosol scattering and absorbing solar radiation, changing the temperature profile that could influence the strength of convection (Chou 2005). The indirect effect is based on which aerosols interact with surrounding precipitations including the effects from the aerosol altering radiation balance associated with cloud microphysics (e.g., Gettlelman et al. 2008) and invigorates vertical cloud development. Enhanced melting and evaporative cooling at lower levels also influence precipitation. Prior studies analyze the aerosol invigoration effect through modeling and found more latent heat is released by condensation, creating a positive feedback of enhanced buoyancy and stronger updraft (Khain et al. 2005; Wang 2005;; Fan et al. 2007;

Tao et al. 2007;; Fan et al. 2009; Van Den Heever et al. 2011). Li et al. (2011) conducted an analysis of seasonal variation and found this effect to be more pronounced during the summer season and more favorable for the invigoration effect owing to strong convection. In the colder season, by contrast, there are less likely to be thermally driven convective clouds. Multiple studies (e.g., Rosenfeld and Lensky 1998; Khain et al. 2005; Rosenfeld et al. 2008; May et al. 2009, 2011) point to a positive relationship between cloud formation in an aerosol-rich environment and storm invigoration. The observational work of May et al. (2011) using polarimetric weather radar observations indicated that a high aerosol environment results in a lower concentration of large drops especially for high reflectivity bins (40 dBZ and higher) because higher reflectivity implies higher rain and collision rates. This should also result in a higher Z_{DR} value. Wilson et al. (2011) conclude that during the early growth stage of a storm, the aerosol concentration depends on various meteorological factors and aerosol-source characteristics that vary by location and time. It is also well known that CCN associated with continental aerosols may alter microphysical processes, leading to higher cloud drop concentration and smaller mean cloud droplet size (e.g., Lohmann et al. 2003).

Simulations performed by Fan et al. (2013) indicate that aerosol particles can influence deep convective clouds by altering the cloud properties via the indirect microphysics effect. Aerosol also leads to the ubiquitous invigoration of convective storm updrafts, which numerous studies have observed (e.g., Bell et al. 2008; Bell et al. 2009; Yuan et al. 2011; Altaratz et al. 2014). However, Fan et al. (2013) indicated that in some cases aerosol might not invigorate convection, and the actual result is highly dependent on the environmental conditions, especially wind shear. Hence, a thorough analysis is required

to incorporate aerosol thermodynamic and microphysical effects to examine the aerosol impact on storm properties. Rosenfeld (1999) conducted satellite observations comparing the cloud temperature and droplet effective radius between clean and smoky environments and discovered that in the clean environment droplet radius achieved a threshold value of 0.014 mm at a temperature of -8°C, while in a smoky environment, that threshold was not reached until -12°C. This indicates the precipitation layer (the zone in which precipitation-sized cloud droplets grow) has been suppressed and smaller droplets are lifted to higher altitude in the smoky environment. The smoky environment also causes cloud droplets to be smaller and thus have smaller coalescence efficiency. Li et al. (2011) found that delaying precipitation initiation to above the freezing level would allow conversion of more raindrops to ice hydrometeors, resulting in larger latent heat release. Kalina et al. (2014) compared CCN concentration using four different environmental soundings and discovered that changes in cold pool characteristics as a function of CCN concentration are nonmonotonic and highly dependent on environmental variables. The microphysical processes (e.g., collision-coalescence) that directly involve cloud droplets are most significant when CCN concentration is between 2000 – 3000 cm^{-3}, while microphysical process rate changes as a function of CCN concentration are less sensitive beyond CCN concentration of ~3000 cm^{-3}. This further suggests that the extreme concentration of CCN may not be necessary to perturb the microphysical processes substantially (Figure 2.4).

Several previous works also suggest a positive relationship between aerosol concentration and storm invigoration (e.g., Khain et al. 2005; Bell et al. 2008; Lee 2011; Tao et al. 2012; Clavner et al. 2018; Lebo 2018), however, an observational study including the

aerosol effect and the effects of environmental conditions on continental thunderstorms across a wide range of CCN concentration has not been conducted (e.g., including mean droplet sizes shortly after convection initiation and depth of the differential reflectivity column across a wide range of environments). The research described in this thesis is focused on aiding operational/research meteorologists by providing supplemental observational evidence for effects of CCN on early deep convective storms.

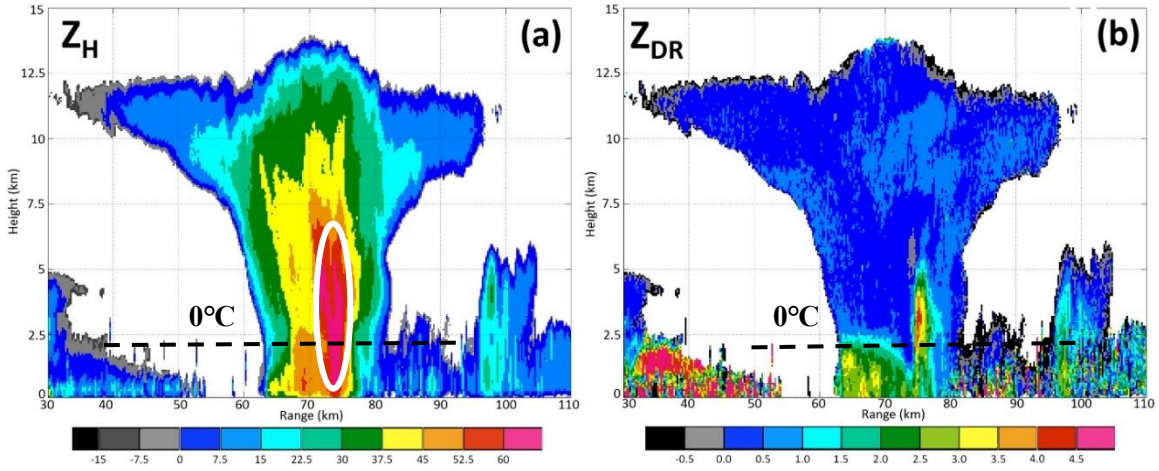

Figure 2.1: An example of a Z_{DR} column (white oval) associated with the reflectivity core (left). The data were collected by the Norman, Oklahoma, radar (KOUN) at 0523 UTC on 27 Apr 2013 along the 144° azimuth (from Kumjian 2014, Fig. 1).

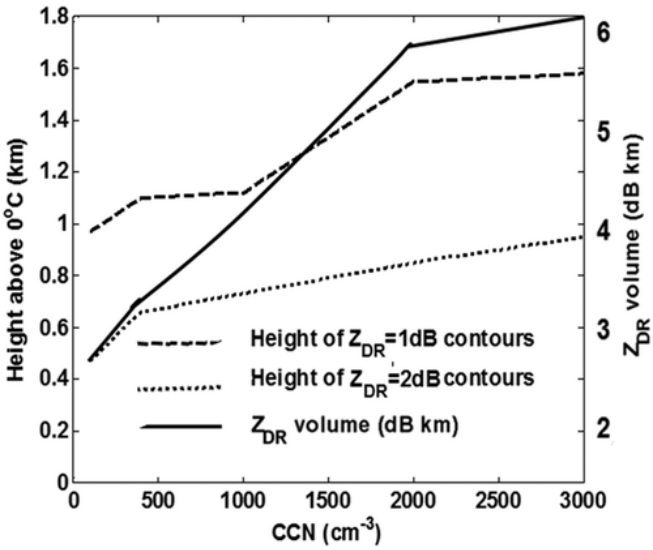

Figure 2.2: Dependencies of time-averaged heights of the maximal elevations of Z_{DR} = 1- and 2-dB contours and time-averaged Z_{DR} column volume on CCN concentration determined at 1% supersaturation (from Ilotoviz et al. (2018), Fig. 18).

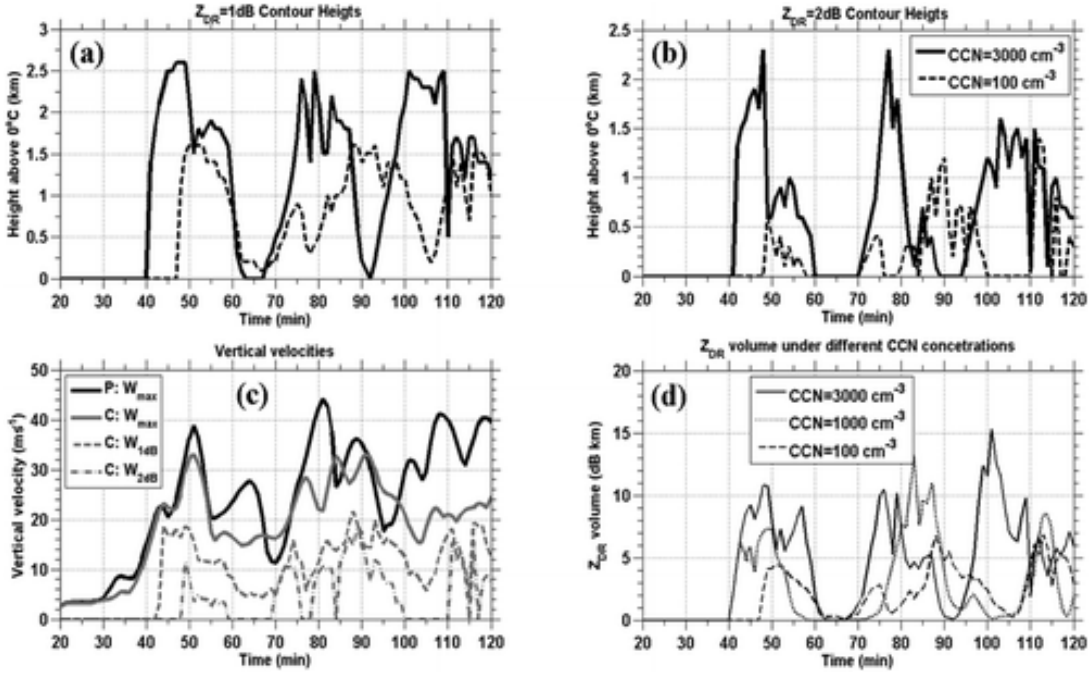

Figure 2.3: Time dependence of the maximum elevations of the contour Z_{DR} = 1 and 2 dB above the unperturbed environmental 0°C isotherm at CCN concentration of 3000 cm^{-3} (solid line) and 100 cm^{-3} (dashed lines) (from Ilotoviz et al. (2018), Fig. 17).

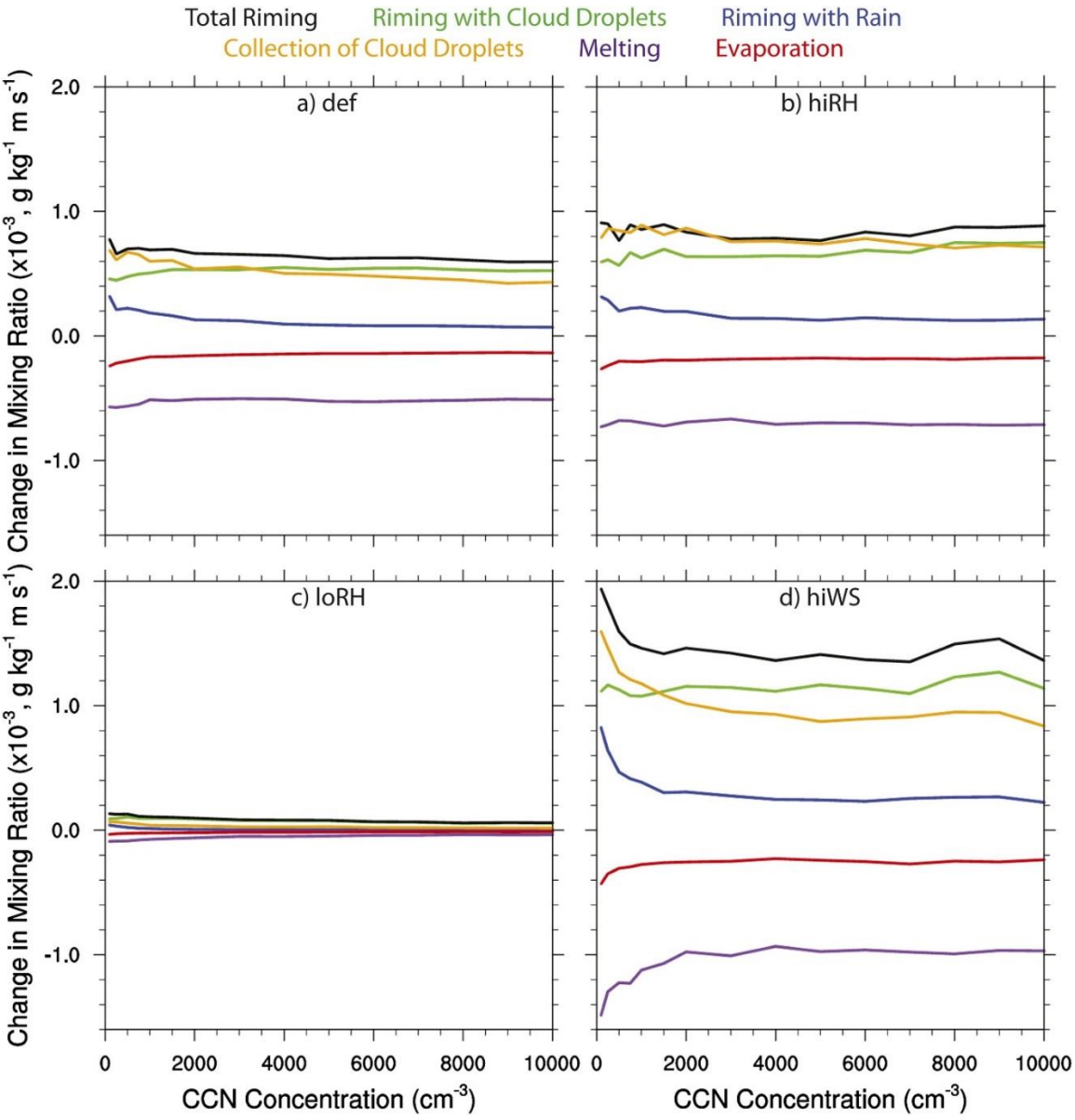

Figure 2.4: Vertically integrated, horizontally averaged microphysical process rates vs. CCN concentration at time = 120 minutes for (a) default sounding, (b) high relative humidity sounding (c) low relative humidity sounding and, (d) high vertical wind shear sounding (from Kalina et al. (2014), Fig. 11).

3. Methodology

I. Thunderstorm Case Selection

One of the primary tasks of this study was to identify a set of thunderstorms influenced by different aerosol concentrations. Polarimetric radar observations from the Weather Surveillance Radar-1988 Doppler (WSR-88D) at Vance Air Force Base, Oklahoma (KVNX) were used to identify the microphysical structure of thunderstorms. Thunderstorms during the period from 2011 to 2017 were selected for analysis if they were within the effective range of KVNX ($\leq$ 75 km for mean droplet size; $\leq$ 100 km for Z_{DR} column depth) and closely associated with a representative proximity sounding, which was an initialization from the Rapid Update Cycle or Rapid Refresh (RUC/RAP). Times when thunderstorms occurred were screened for frontal boundaries relative to the location of the model output soundings (RUC/RAP) in order to adequately represent the nearby environment. The model output sounding within 80 km was an effective representative of the near-storm environments within an hour timeframe (Potvin 2010). Two model soundings were averaged to obtain a representative environment if the analysis period was greater than one hour in length (e.g., Van Den Broeke 2016). Hourly model output from RUC/RAP has finer spatial and temporal resolution compared to the upper air observation network in the United States as described by Thompson et al. (2003). However, RAP output can contain biases including conditions being too cool and dry at the surface, being too warm and moist at lower levels, and tending to overestimate tropospheric wind speed by 1 - 2 m s^{-1} (Benjamin 2016). Although the mixed layer convective available potential energy (MLCAPE) can be overestimated, the error was

unlikely to have a severe impact on the operational evaluation of storm environments (Thompson et al. 2003).

A dataset consisting of 36 thunderstorm cases with polarimetric radar data was used to test if CCN concentration variability is associated with differences in droplet size characteristics. Thunderstorms were selected only if they initiated within the observing range (≤ 75 km from the KVNX radar, Figure 3.1, red circle). The time of convection initiation was defined as the lowest volume scan 15-20 minutes after radar reflectivity ≥ 20 dBZ was first observed, following May et al. (2011). Thunderstorms which first initiated outside the observing range (≥ 75 km from the radar) but moved through the observing range in its dissipating stage and storms that are embedded within the convective region are excluded from the analysis. The differential reflectivity data threshold between 0 to 6 dB was chosen to correspond to droplet sizes in light to moderate rain, following guidance by the National Oceanic and Atmospheric Administration (NOAA) Warning Decision Training Division (WDTD 2013). Data were exported to a shapefile which could be analyzed in ArcGIS. The associated shapefile contains the relevant Z_{DR} value and coordinates for each pixel (Figure 3.3). The clipping tool from ArcGIS was applied to obtain Z_{DR} pixel coordinate information for the sample of Z_{HH} pixels ≥ 20 dBZ, thus each Z_{DR} pixel has the same coordinate as Z_{HH}. Candidate Z_{DR} pixel was selected 0.5 km above LCL and CCL, then averaged (Figure 3.4). The lifting condensation level (LCL) or convective condensation level (CCL) was required to be greater than 15℃ for this dataset as aerosol effects are more apparent in clouds with warm bases (Rosenfeld and Bell 2011).

Z_{DR} column height associated with 66 thunderstorm cases was examined to test if the high aerosol concentration was associated with updraft invigoration. Since the aerosol effect can depend on environmental characteristics, Z_{DR} column variability was compared to environmental distributions of wind and instability variables. Since the Z_{DR} column height was not stable until during the mature stage of the storm life cycle, thunderstorm cases for a comparison between CCN concentration and mean Z_{DR} column height was selected when the Z_{DR} column first showed up after storm initiation and averaged throughout the analysis window until it disappeared or move outside the observed range (100 km, Figure 3.1 blue circle). This method was also consistent with the observing range of Van Den Broeke (2016). The Z_{DR} column height was identified as illustrated by Van Den Broeke (2017) using the altitude at the top of the 1-dB Z_{DR} column subtracted from the altitude of the ambient 0°C level (Figure 3.5). This was consistent with the 1-dB threshold used by the Snyder et al. (2015) Z_{DR} column algorithm. As noted by Van Den Broeke (2017), this technique assumes that the Z_{DR} column top is located at the beam centerline of the highest tilt at which the column appears, which can be subject to significant error due to vertical beam widening at longer range. Storms were discarded if they moved beyond 100 km from the radar or if radar data were not available. Characteristics of the thunderstorms were also compared to a CCN dataset (discussed in the following section); a case was discarded if radar or CCN data were missing. A complete list of cases is included in Table 3.1.

II. Cloud Condensation Nuclei Quantification

In this study, data from the Southern Great Plains (SGP) site of the Atmospheric Radiation Measurement (ARM) Climate Research Facility in Lamont, Oklahoma, are

used to represent the near-surface CCN concentration of the thunderstorm environment. The ARM data location is approximately 59 km southeast of KVNX and approximately 42 km northeast of Enid, OK, where the model sounding is located (Figure 3.2). The SGP site was the first field measurement site established by the ARM and offers high-quality data from well-maintained instrumentation (Department of Energy 2018). The CCN particle counter measures the concentration of aerosol particles by drawing an air sample through a supersaturated column (Department of Energy 2018), leading to condensation onto aerosol particles. Particles that are activated are counted and sized by an optical particle counter (OPC). CCN data are recorded after every sample. As an example, Figure 3.2 shows total particle count for 20 May 2011; each peak indicates hourly CCN concentration as a function of supersaturation percent (SS%), with values at the top of each peak indicating the activated particle number concentration at 1% SS. It is generally agreed that peak supersaturation in convective clouds is below 1% in the absence of precipitation (e.g., Song et al. 1989; Kalina et al. 2014). Devenish et al. (2016) indicate that the maximum supersaturation is about 0.2% in stratocumulus and close to 0.5% or greater in cumulus clouds; However, supersaturation unlikely exceed 1%–2% in warm clouds except for vigorous convective clouds. Thus, the concentration of CCN at 1% supersaturation was used in our studies consistent with empirical dependence (equation 1) and simulation studies of midlatitude storms (e.g., Ilotoviz et al. 2015, 2018). The CCN count was based from the nearest 1% peak prior to the observation time; each thunderstorm was also checked for its local environment to ensure the CCN count was not influenced by outflow boundaries or other small-scale influences. CCN datasets which were incomplete were discarded. The entire 2016 dataset was excluded because it

contained questionable results caused by an error in the OPC (U.S. Department of Energy Office of Science 2018). This problem resulted in CCN counts larger than the CN counts, indicating that CCN counts were too high. The overall CCN concentration at Lamont, Oklahoma, shows widely varying CCN number concentration ranging from 60-5000 cm^{-3} which may play an important role to alter microphysical structure in regional thunderstorms. The overall CCN dataset agrees with observations by Kalina et al. (2014) who observed CCN concentration in Great Plains supercell environments from 200-5000 cm^{-3}.

III. Differential Reflectivity Calibration

Another necessary task was to reduce the Z_{DR} calibration error since the polarimetric variable Z_{DR} was used to identify the raindrop characteristic distribution and the Z_{DR} column height. Z_{DR} has first introduced over 40 years ago and has been known to be problematic on the WSR-88D network (e.g., Zrnić et al. 2006; Van Den Broeke 2016). Z_{DR} calibration continues to be an issue for the WSR-88D radar network, and its temporal stability is poorly documented. Earlier Z_{DR} calibration techniques were developed by Gorgucci et al. (1992), who found that Z_{DR} can be calibrated using the properties of the polarimetric measurements in the rain. Their method allowed calibration to be obtained from radar measurements collected during the operational routine. However, this technique assumes the Z_{DR} is independently calibrated (Bechini et al. 2008). Another method introduced by Zrnić et al. (2006) uses a different approach to estimate Z_{DR} calibration that does not rely on the properties of the scatterers. The meteorologist working with a Z_{DR} dataset from the WSR-88D network should be aware of the error

caused by calibration offset and is encouraged to review prior studies about reducing/minimizing Z_{DR} error.

In this study, the Z_{DR} calibration method follows that implemented by Picca and Ryzhkov (2012) since deep convection was present in all datasets. First, Z_{HH} values were selected between 20 – 35 dBZ approximately 1.5 km above the environmental freezing level. Unreliable data such as differential attenuation were excluded. Scatterers associated with Z_{HH} between 20 – 35 dBZ at this altitude are assumed to be dry snow aggregates, which have a known mean Z_{DR} value of approximately 0.15 dB (Picca and Ryzhkov 2012). All Z_{DR} pixel values within the region with good Z_{DR} data were averaged, and the mean value was subtracted from the expected value of 0.15 dB to get the Z_{DR} calibration factor. The calibration factor was added/subtracted from the original Z_{DR} value when Z_{DR} was used to identify radar features described herein (Figure 3.4). The mean value of the calibration factor for the overall radar dataset is 0.225 dB, with bias > 0.2 dB in 60.6% of events and > 0.3 dB in 16.3% of events.

IV. Polarimetric Radar Variables used to Infer Raindrop Characteristics and Z_{DR} Column

A primary objective of this study was to identify how raindrop characteristics vary as a function of CCN concentration. Many prior studies (e.g., Blanchard 1980; Wurzler et al. 2000; Khain et al. 2005; Seifert and Beheng 2006; van den Heever et al. 2006; Li et al. 2011) hypothesized that in higher aerosol concentration environments, thunderstorms will have vertical drop size distribution (DSD) and concentration differences above the freezing level relative to low-aerosol environments because the aerosol can change the rate of cloud microphysical processes, modifying the latent heating/cooling and altering

the local temperature and moisture profiles. Since raindrop characteristics can be substantially altered by CCN, it is hypothesized that mean Z_{DR} values will be reduced at low levels and increased in the upper levels of thunderstorms early in their life cycles in polluted environments.

Since the storms that were analyzed occurred in a variety of environments, implementing some commonly used environmental parameters across the 36 storms can clarify whether a trend was apparent for certain environments and whether such ideal application should be useful over a large range of deep convective environments. Values representative of the near-storm environment were obtained, averaged and calculated from RAP (n = 31)/RUC (n = 5) model soundings. The CCN concentration varied from 67.38 cm^{-3} to 4743 cm^{-3}, with values for most storms ~1000-3000 cm^{-3}. Cases with CCN concentration $\leq$ 800 cm^{-3} were considered clean (following Tao et al. 2007). Low-CCN cases may be unrepresentative of the microphysical process in midlatitude storms. Hence, this resulted in fewer cases for analysis (n = 31). This range of observed CCN concentration is representative of the spectrum of convective environments in this region (Kalina et al. 2014). The height of the freezing level typically ranged from ~2.8 km to 4.5 km. Most unstable convective available energy (MUCAPE) varied from ~200 J kg^{-1} to near 3650 J kg^{-1}. The raindrop characteristics inferred by polarimetric radar observations were compared to environmental distributions of wind and moisture to characterize the variation in these characteristics across a wide range of environmental aerosol concentration, shear, instability, and height of the freezing level (e.g., Van Den Broeke 2016).

Aerosols within the thunderstorm inflow suppress the warm rain processes, invigorating intense ice precipitation processes may lead to the formation of hail above the freezing level (e.g., Dagan et al. 2015). Hence, it is hypothesized that updraft signatures (Z_{DR} columns) will be more pronounced as the updraft deepens through the mature phase. Among sample of storms analyzed for Z_{DR} column, the aerosol concentration varied from 67.4 cm^{-3} to ~3700 cm^{-3}, with values for most storms ~1500-3000 cm^{-3}. This range covers the spectrum of convective environments. The height of the freezing level ranged from ~2.8 km to ~4.6 km. MUCAPE varied from ~280 J kg^{-1} to near 5600 J kg^{-1}. Finally, the effective storm relative helicity (ESRH) varied from -113 to 478 m^2 s^{-2}. The differential reflectivity column characteristics inferred by polarimetric radar observations are compared to work performed by Van Den Broeke (2016). Van Den Broeke (2016) described the difference in Z_{DR} column characteristic across a variety of environments for supercell storms. The goal here is to describe the differences of Z_{DR} column depth across a range of environments and CCN concentrations to see which plays the dominant role.

Table 3.1: Date and analysis window for mean Z_{DR} (CCN > 800 cm^{-3}, 31 cases) and Z_{DR} column depth (66 cases). All storms occurred in the domain of KVNX.

Date	Analysis Time (Mean Z_{DR})	Analysis Window (Z_{DR} column depth)
20 May 2011	0518	N/A
23 May 2011	2031	2018 – 2057
24 May 2011	N/A	2034 – 2053
11 June 2011	N/A	2203 – 2221
12 June 2011	N/A	0242 – 0259
20 June 2011	N/A	2242 – 2255
03 July 2011	N/A	2227 – 2237
24 July 2011	N/A	2301 – 2310
29 July 2011	2040	2055 – 2105, 2229 – 2239
03 August 2011	NA	2309 – 2324
07 August 2011	NA	2153 – 2208
12 August 2011	1030	1005 – 1045
13 August 2011	N/A	0004 – 0027
17 August 2011	2137	2212 – 2237
01 May 2012	N/A	0028 – 0110
19 May 2012	N/A	2309 – 2331
29 May 2012	N/A	2131 – 2209
31 May 2012	N/A	0217 – 0221
06 June 2012	1145	N/A
16 June 2012	N/A	1021 – 1026
17 June 2012	0130	0116 – 0158
09 July 2012	N/A	2001 – 2037
10 July 2012	0208, 0904	N/A
24 August 2012	0859	N/A
05 June 2013	N/A	0613 – 0640
16 June 2013	2303	N/A
11 July 2013	N/A	0652 – 0659
16 July 2013	N/A	2329 – 2342
18 July 2013	N/A	0010 – 0015
21 July 2013	N/A	0141 – 0155
29 July 2013	N/A	2303 – 2316
05 August 2013	N/A	2256 – 2303
08 August 2013	N/A	0620 – 0634
09 August 2013	N/A	0511 – 0520
12 August 2013	N/A	0733 – 0737
13 August 2013	N/A	0201 – 0214
16 August 2013	N/A	0214 – 0231
09 May 2014	N/A	0231 – 0243

22 May 2014	N/A	2036 – 2044
03 June 2014	0018	0034 – 0050
24 June 2014	N/A	2209 – 2224
01 July 2014	N/A	0611 – 0616
18 August 2014	2041	2111 – 2121, 2210 – 2220
19 August 2014	N/A	0034 – 0040
26 August 2014	N/A	2059 – 2107
28 August 2014	N/A	2350 – 2357
29 August 2014	2012	2007 – 2026
04 May 2015	2015	N/A
06 May 2015	2004	1006–1016, 2051–2111, 2241–2251
07 May 2015	1942	0049 – 0110, 2013 – 2037
08 May 2015	2138	N/A
09 May 2015	N/A	1629 – 1634
10 May 2015	N/A	1327 – 1346
16 May 2015	N/A	1017 – 1026, 1628 – 1633
26 May 2015	1933	N/A
27 May 2015	N/A	0038 – 0058
08 June 2015	N/A	0013 – 0034
12 June 2015	N/A	0411 – 0421
13 June 2015	N/A	0028 – 0033
15 June 2015	0037	0115 – 0124
26 June 2015	0924	N/A
02 July 2015	0017	0047 – 0057
03 July 2015	0200	0235 – 0243
17 July 2015	N/A	0301 – 0314
23 July 2015	N/A	0820 – 0840
29 July 2015	2117	2145 – 2210
30 July 2015	N/A	1202 – 1207
09 August 2015	1452	N/A
14 August 2015	1047	N/A
19 August 2015	0423	0428 – 0443
22 August 2015	N/A	0840 – 0901
10 May 2017	1850	N/A
11 May 2017	1758	N/A
27 June 2017	0448	N/A
02 July 2017	1920	N/A
07 July 2017	2353	N/A
14 July 2017	2017	N/A
05 August 2017	2111	N/A
16 August 2017	2256	N/A
20 August 2017	0020	N/A

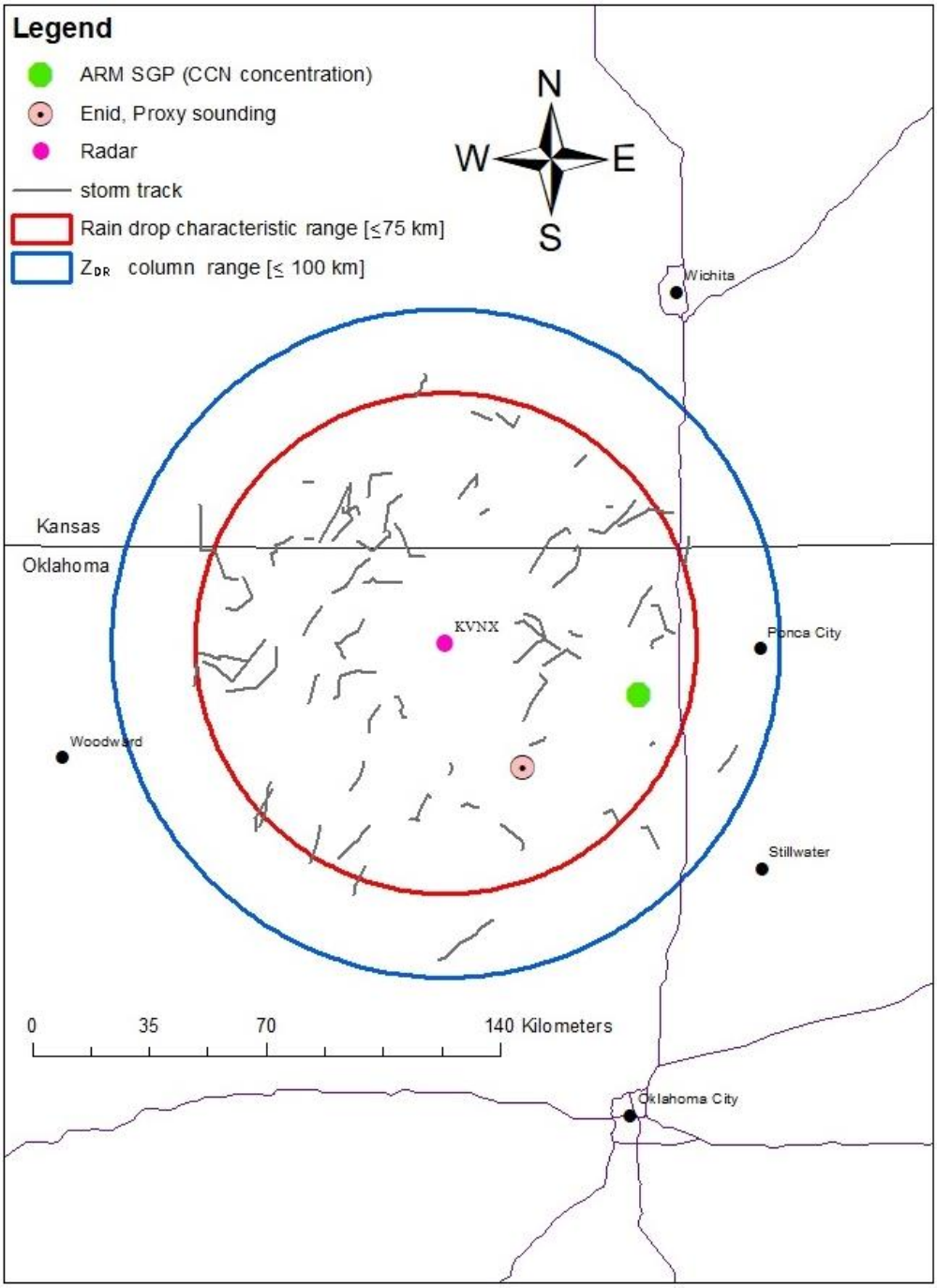

Figure 3.1: The location of the radar, the radar range ring and the analysis area of droplet size distributions and the Z_{DR} column depth. ARM CCN site (red dot), 100 km from KVNX for Z_{DR} column depth (blue circle), and 75 km from KVNX for mean Z_{DR} range (red circle).

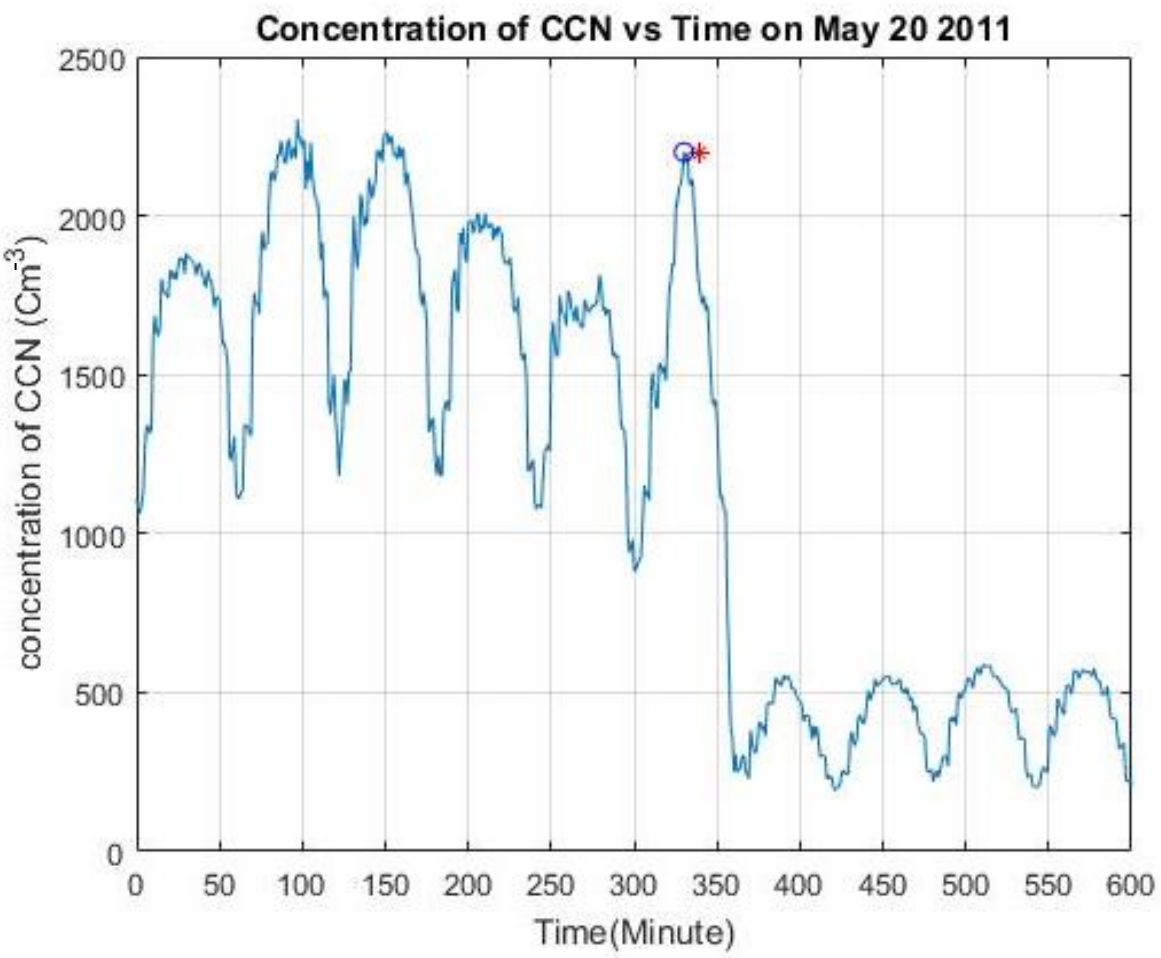

Figure 3.2: Time series of CCN concentration on 20 May 2011. Each subpeak indicates CCN concentration for supersaturation% (SS %) values of 0.0%, 0.1%, 0.2%, 0.5%, 0.8% and 1%. The highest peak at each hour represents the CCN concentration at 1% SS. The red dot indicates the radar observation time frame for mean Z_{DR} and blue circle indicates CCN count that was used.

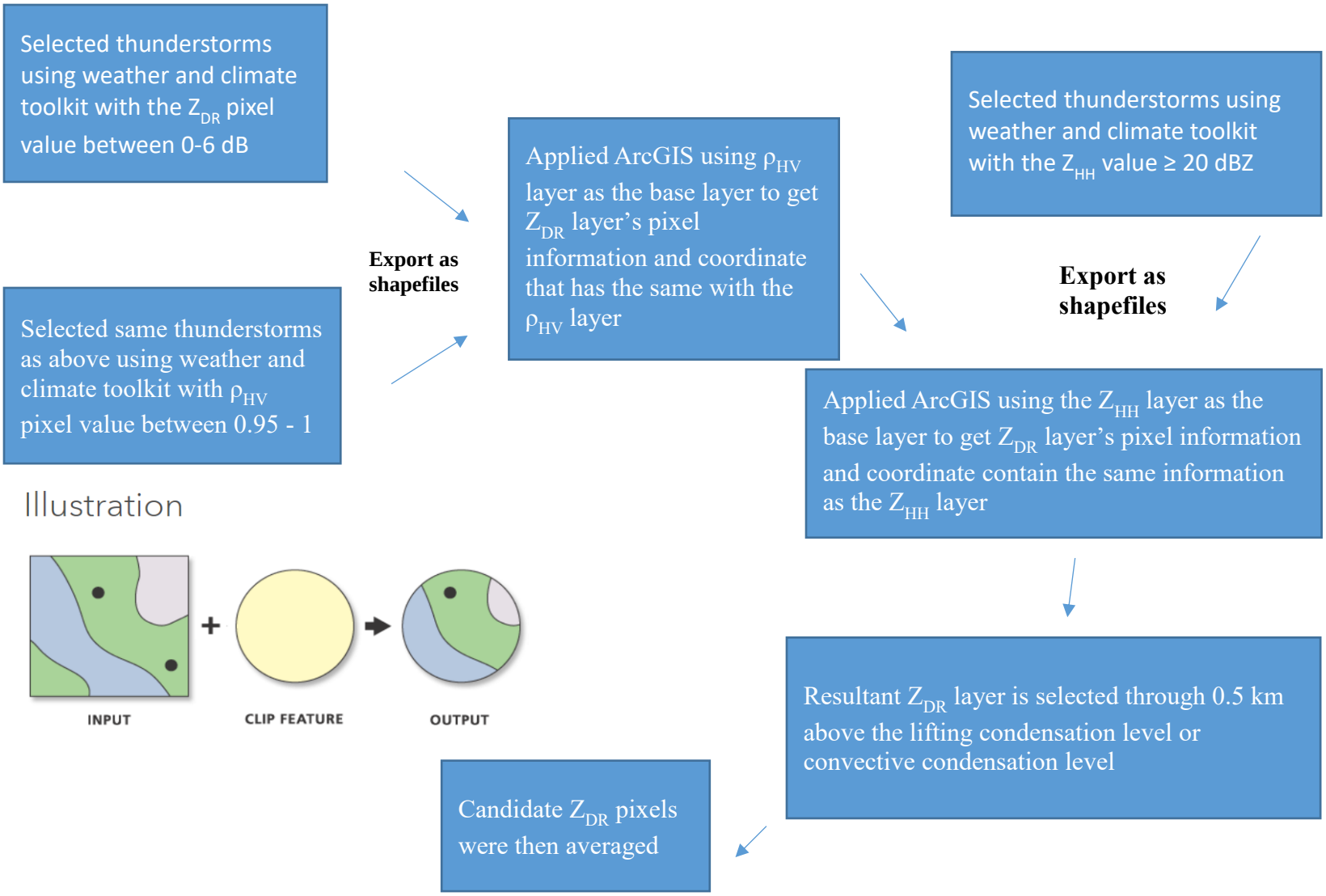

Figure 3.3: Flowchart of polarimetric radar variables used to calculate Z_{DR} raindrop characteristics, illustration image provide by ESRI)

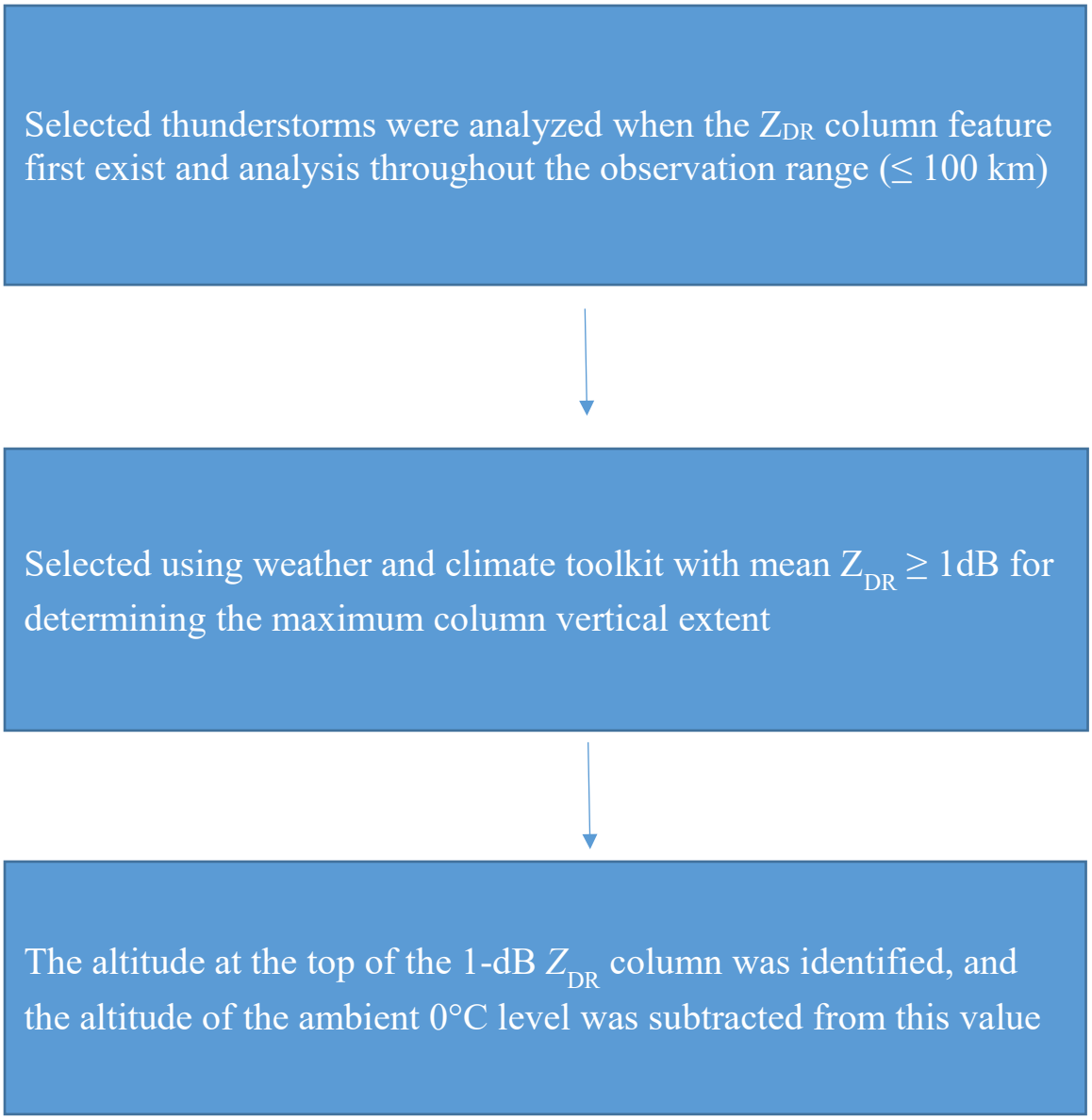

Figure 3.4: Flowchart of polarimetric radar variables follow Van Den Broeke (2016) used to estimate the Z_{DR} column height.

4. Aerosol Concentration Effects on the Distribution of Drop Size soon after Convection Initiation

The mean differential reflectivity (hereafter referred to as 'mean Z_{DR}') is estimated 0.5 km above cloud base during the early storm stage (15 to 20 min after convection initiation). The 36 thunderstorm cases were selected from the warm season (May to August) within the domain of KVNX in northwestern Oklahoma. The correlation coefficient is used herein to ensure the data included are dominated by liquid droplets (WDTD 2013). Pixels used to calculate the mean Z_{DR} were selected to overlap the copolar correlation coefficient between 0.95 – 1 to ensure that the droplets were mostly uniform and not mixed with other particle species. Since the analysis time was shortly after convection initiation, $\rho_{HV} < 0.95$ likely indicates mixed precipitation types or biological scatter, while $\rho_{HV} > 1.0$ are caused by low signal to noise ratio. Therefore, pixels with those values are removed in our analysis. This increases confidence in the results presented here as it allows for removal of contaminated data (e.g., particle other than liquid droplets, biological scatter. Most of the ρ_{HV} values are close to 1.0, indicating the observed data are mostly uniform and with few data points below 0.95 (Figure 4.1) The mean Z_{DR} approximate range (1.48 to 3.87 dB) corresponds to mean drop diameter of 2.19 - 3.50 mm. This was estimated based on Bringi et al. (1998) who use power-law relations based on disdrometer observations and drop shapes for $Z_{HH} < 35$ dBZ and $Z_{DR} \geq 0.2$ dB. Radar metrics were compared to aerosol data and environmental variables from RAP/RUC soundings to examine whether environmental variables or aerosol variability is more influential on droplet size, and to examine the relative importance of each effect.

Then, a predictive equation was developed for mean Z_{DR} using multiple linear regression which uses aerosol concentration and environmental variables as predictors (Table 4.1) There is a negative correlation between CCN concentration and mean Z_{DR} (r = -0.228) between moderate (500 cm^{-3}) to high CCN concentration (5000 cm^{-3}) and positive correlation associated with MUCAPE (r = 0.268). Environmental variables (freezing level, lifting condensation level (LCL) temperature and 0-3 km shear) have a weak correlation to mean Z_{DR} (Table 4.1). Prior observations and simulations did not find robust evidence for how each environmental parameter was correlated with CCN concentration. How CCN concentration affects storms under different environmental conditions is poorly documented, and the results can vary depending on the conditions described by Altaratz et al. (2014). Such problems still pose challenges for numerical modeling and observations.

Since surface heating leading to pre-afternoon thunderstorm is frequent during the warm season in the Great Plains, the convective condensation level (CCL) was used as a reasonable estimate of cloud base height when air parcels were rising due to heating from the surface (6 cases). The LCL was used to estimate of cloud base height when air parcels experienced forced ascent (30 cases; National Weather Service 2018). LCL was used if there was a front within the observation range (≤ 100 km); otherwise, the CCL was used. Hence, the mean Z_{DR} layer is measured from cloud-base (CCL or LCL) up to 0.5 km above the cloud base. The distribution of mean Z_{DR} values varies from 1 to 3 dB between CCN concentration of 500 cm^{-3} and ~5000 cm^{-3} (Figure 4.2a). Although Pearson's correlation indicates a weak association between these variables (r = -0.228), the overall distribution trends toward higher Z_{DR} values associated with lower CCN

concentration and indicates that the distribution shifts towards larger droplet size with lower CCN concentration (Figure 4.2a). This suggests that fewer aerosols may be associated with larger droplets within 20 min of convection initiation. This trend is also consistent with prior findings which used simulations and found larger droplet size in low aerosol environments ~20 min after observed convection initiation (Koren et al. 2005; Seifert and Beheng 2006; Fan et al. 2007; Van Den Heever et al. 2011).

The area occupied by reflectivity ≥ 40 dBZ was extracted for separate analysis of mean Z_{DR} associated with stronger updraft regions. This threshold followed previous research classifying the convective environment (e.g., Matyas, 2009; Goudenhoofdt and Delobbe, 2013).

When the Z_{DR} region was selected based on $Z_{HH} \geq 40$ dBZ, The relationship is stronger (Pearson's correlation = -0.365) than when using the lower Z_{HH} threshold (≥ 20 dBZ). The high-Z_{HH} regions indicate the approximate location of the strong updraft and are hypothesized to be where vertical transport of droplets is enhanced within the cloud, resulting in delayed raindrop formation and prevention of larger droplets from falling through the layer and weakening the updraft (e.g., Rosenfeld 1999, 2000). It also promotes size sorting, and thus trends of droplet-size characteristics as a function of aerosol concentration are hypothesized to be more apparent. It should also be noted that in some cases a weak reflectivity core can occur in strong storm updrafts as they carry hydrometeors upwards quickly (NOAA 2018). This should not be a significant issue in this dataset as it can be assessed by examining multiple radar scans during the storm evolution. In addition, the environments in this dataset also have significant difference compared to the supercell environment (Figure 4.8).

Previous observations and simulations by Fan et al. (2009) show the importance of vertical wind shear, which regulates the aerosol loading effect on deep convective clouds. As described by Fan et al. (2009), vertical wind shear can qualitatively determine whether convective strength is enhanced or suppressed due to aerosol effects. Increased aerosols favor storm updraft invigoration under weak wind shear since stronger updrafts support a more effective collision-coalescence process, resulting in larger droplets with larger mean Z_{DR} (Rogers and Yau, 1989). Under strong wind shear, increased aerosol loading will suppress the updraft and lead to a smaller mean Z_{DR}. The aerosol effects described by Fan et al. (2009) are examined in this study. The distribution of 0-3 km wind shear and mean Z_{DR} values (Figure 4.3) in the cases analyzed were weakly correlated ($r = -0.079$) and with large spread between wind shear values of 10 to 20 m s^{-1}. This study shows weak evidence of updraft invigoration in the lower level (mean Z_{DR} layer) under weak wind shear and does not have robust results to support the numerical model results by Fan et al. (2009) in which high aerosol loading was found to suppress convection, resulting in weaker updrafts and lower water content in a strong wind shear environment. This findings also are not consistent with Storer et al. (2010), who ran simulations in which CAPE and aerosol concentration varied. Their results indicated that the high CCN case was associated with lower precipitation for moderate-high wind shear, with a lesser effect at lower wind shear (Figure 4.7). The lower precipitation for moderate-high wind shear corresponded to the suppressed updraft discovered by Fan et al. (2009).

Aerosol indirect effects can result in differences in storm microphysical structure depending on environmental parameters such as CAPE (e.g., Storer et al. 2010). CAPE is

one of the most representative measurements of instability. Instability has a substantial impact on the updraft strength in a storm (for example, simulations by Ilotoviz et al. (2018), in which it was found that lower CCN cases generally had shallower Z_{DR} columns associated with weaker updraft and the higher CCN cases had larger Z_{DR} columns with stronger updraft; Figure 5.5). The hypothesis that there should be a positive relationship between the mean low-level Z_{DR} value and MUCAPE was tested. This hypothesis was based on Lee et al. (2008) in which cases were simulated to study the aerosol effect. Their results showed more intense updrafts in a high CAPE environment resulting in more condensate transported to saturated regions above the freezing level, leading to stronger updrafts. In addition, the aerosol effect also leads to a less efficient collision-coalescence process due to smaller droplet size (e.g., Rosenfeld 1999, 2000) and prolongs the duration of drop growth by diffusion (e.g., Khain et al. 2005; Wang 2005; Martins et al. 2011). This will result in delaying raindrop formation and promoting the column loading of condensed water resulting in larger droplets being lofted above the freezing level. Hence, a high-MUCAPE environment should result in larger droplets forming in the low levels. Moderate to strong positive correlation ($r = 0.530$) was found between the mean low-level Z_{DR} value and MUCAPE (Figure 4.4), consistent with the theoretical expectation that greater droplet size should be associated with higher MUCAPE. A potential explanation for this relationship includes the possibility that the strong updraft in a high MUCAPE environment enhances the collision-coalescence process at low levels, resulting in larger droplets.

Previous studies suggested that the height of the freezing level would determine the relative importance of the warm rain process during the early stage of a storm. A higher

freezing level may indicate more cloud at warm temperature or warmer temperature at cloud base (e.g.,Van Den Broeke, 2016). A weak correlation was found (r = -0.167) with higher Z_{DR} values associated with lower freezing levels (Figure 4.5). The findings are not consistent with those of Koren et al. (2005), Seifert and Beheng (2006), Fan et al. (2007), Andreae (2009), and Van Den Heever et al. (2011) who found that in the warm rain process, more aerosols provide more CCN and produce more and smaller droplets with a narrow size distribution. It is hypothesized that some correlation in the storm cases analyzed here compared to the model simulations may be due to physical observation limitations such as 1) the simulations are better controlled for varying environmental parameters, or 2) the aerosol concentration can vary over short spatiotemporal scales. The observed background environmental parameters include the distributions of MUCAPE and 0-3 km wind shear (Figure 4.6). The association between these variables suggests that higher MUCAPE is present with lower values of wind shear, indicating that for most storms a stronger updraft is associated with weak wind shear. This can potentially influence aerosol loading as described by Fan et al. (2009), who focused on aerosol effects in environments with variable wind shear. According to their work, in a high wind shear environment, increased aerosol loading would lead to suppressed convection as the evaporational cooling is greater than condensational heating. In a weak wind shear environment, increased aerosol will enhance convection until it reaches an optimum aerosol loading because condensational heating can be greater than evaporational cooling, leading to net higher latent heating and therefore to stronger updrafts.

Certain environmental variables can influence the impact of aerosol loading on convective clouds (e.g., MUCAPE, wind shear, instability). A predictive equation for mean Z_{DR} was developed using multiple linear regression from a set of predictors including environmental variables and CCN concentration. The environmental variables selected as possible predictors included all the variables associated with mean Z_{DR} (Table 4.1) or that had been mentioned in prior literature as important relative to aerosol effects. Environmental parameters were checked for collinearity using the condition index, to ensure the information being included was sufficiently different (e.g., Belsley et al. 2005). The value of the condition index should be less than 30 to indicate minor collinearity, and value above this threshold are excluded in a predictive equation (e.g., Belsley et al. 2005; Van Den Broeke 2016). Then, using the stepwise multiple regression to exclude parameters that were not significant ($p \geq 0.05$), a model were developed that explains 29.5% of the variance in mean Z_{DR} (dB):

$$Z_{DR}\text{ (dB) mean value} = 2.56 - 1.7 \times 10^{-4}\,(a) + 2.65 \times 10^{-4}\,(b), \quad (3)$$

Where a is CCN concentration (cm^{-3}), and b is MUCAPE ($J\ Kg^{-1}$). CCN concentration is negatively correlated to this metric because higher CCN concentration results in higher droplet concentration with smaller mean droplet size (May et al. 2011). Mean Z_{DR} is positively correlated to MUCAPE because a high-MUCAPE environment results in more condensate transported above the freezing level, leading to a stronger updraft. The aerosol effect leads to a less efficient collision-coalescence process due to smaller droplet sizes and narrower drop-size distribution, prolonging the duration of drop growth solely by diffusion. This results in delayed raindrop formation and promotes the

column loading of condensed water, resulting in large droplets being lofted above the freezing level. Therefore, a high-MUCAPE environment with high CCN concentration should result in larger droplets and higher mean Z_{DR} in the low levels.

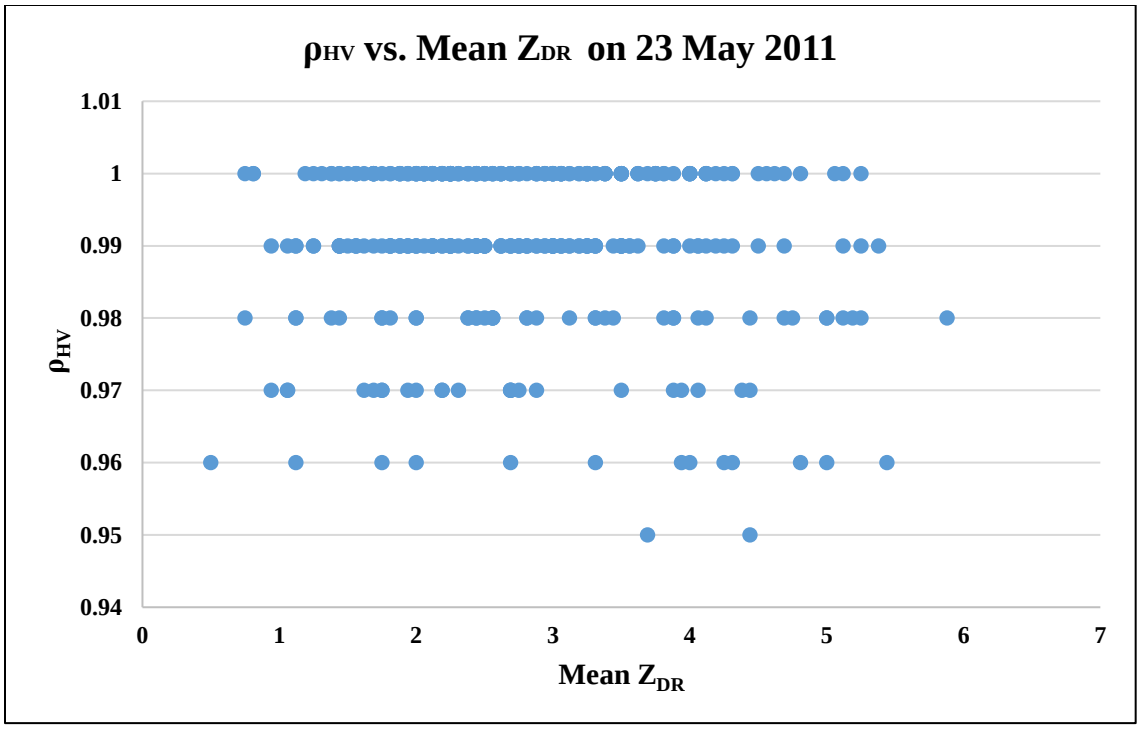

Figure 4.1: ρ_{HV} vs. Z_{DR} for each selected pixel for the 23 May 2011 case. Most observed data points are close to 1 with few data point below 0.97, indicating relatively homogeneous liquid drops.

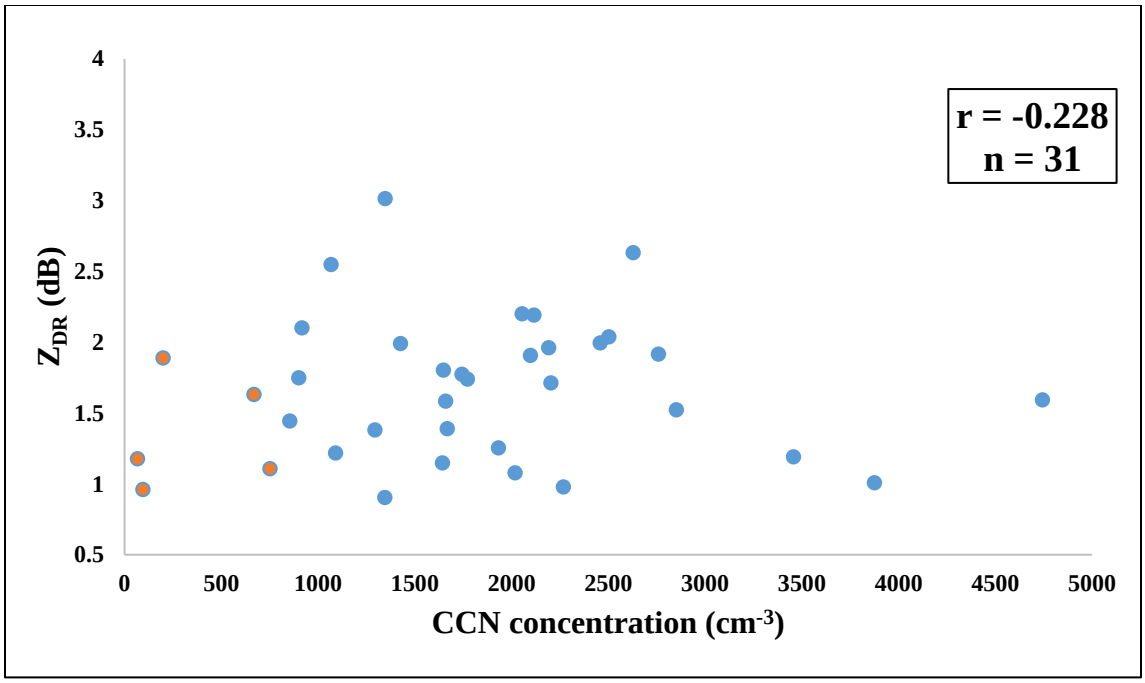

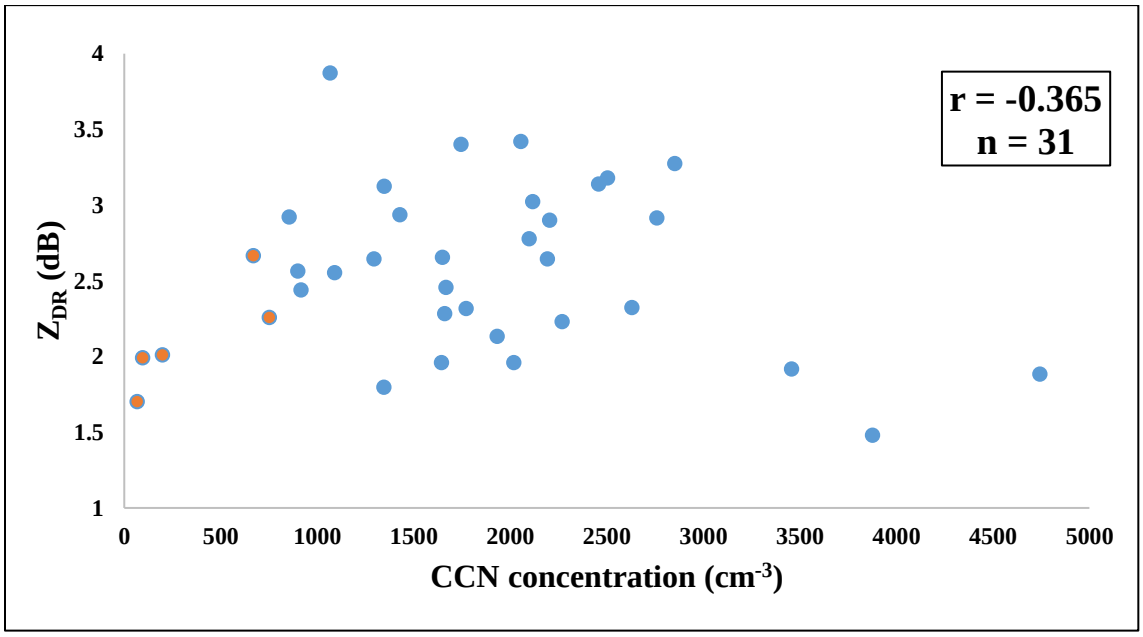

Figure 4.2 Z_{DR} versus CCN concentration using (a) a threshold of $Z_{HH} \geq 20$ dBZ and (b) a threshold of $Z_{HH} \geq 40$ dBZ. As CCN concentration increases (≥ 800 cm^{-3}, blue dot), the Z_{DR} value decreases slightly, CCN concentration increases (≤ 800 cm^{-3}, orange dot), the Z_{DR} value increases. Orange dot (CCN ≤ 800 cm^{-3}, 5 cases) is excluded for r value.

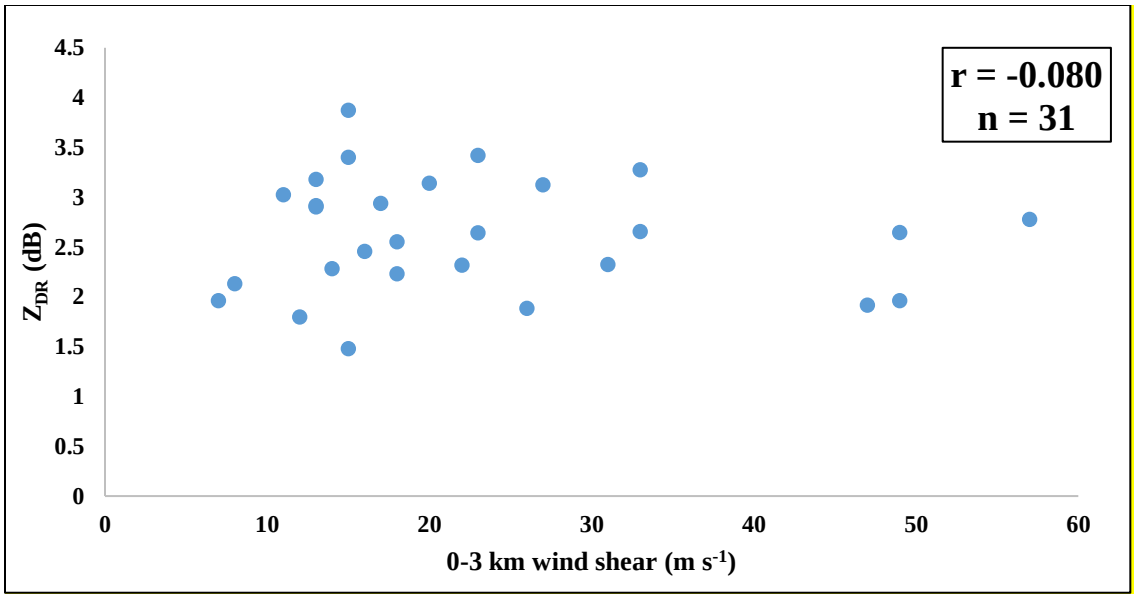

Figure 4.3 Scatterplot for mean Z_{DR} (dB) versus 0-3 km wind shear (m s^{-1}).

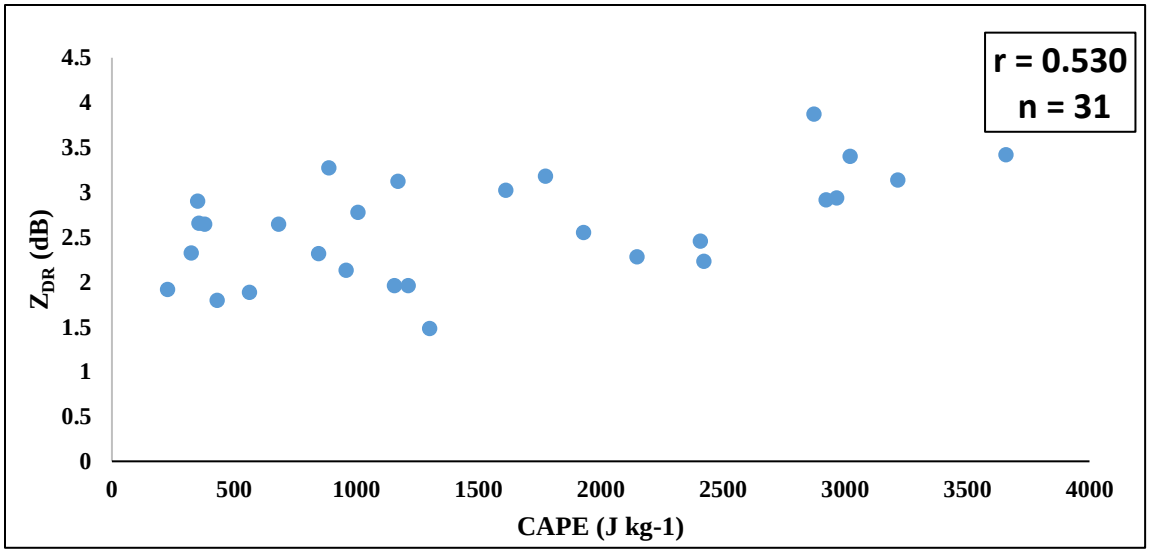

Figure 4.4 Scatterplot for mean Z_{DR} (dB) versus MUCAPE (J Kg^{-1}).

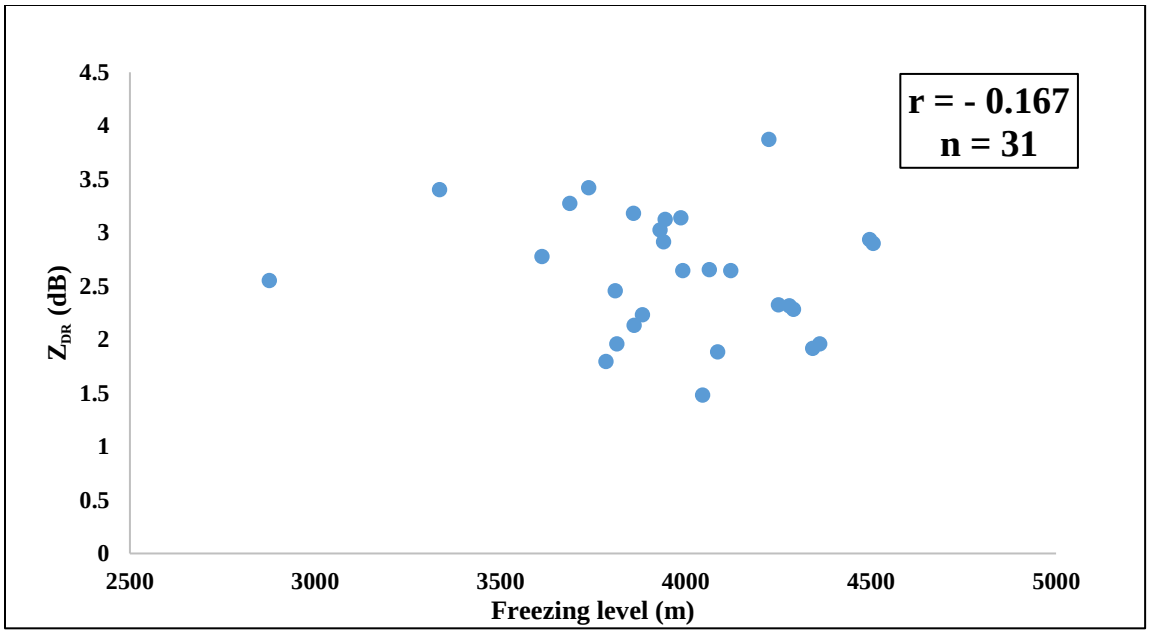

Figure 4.5 Scatterplot for mean Z_{DR} (dB) versus freezing level (m).

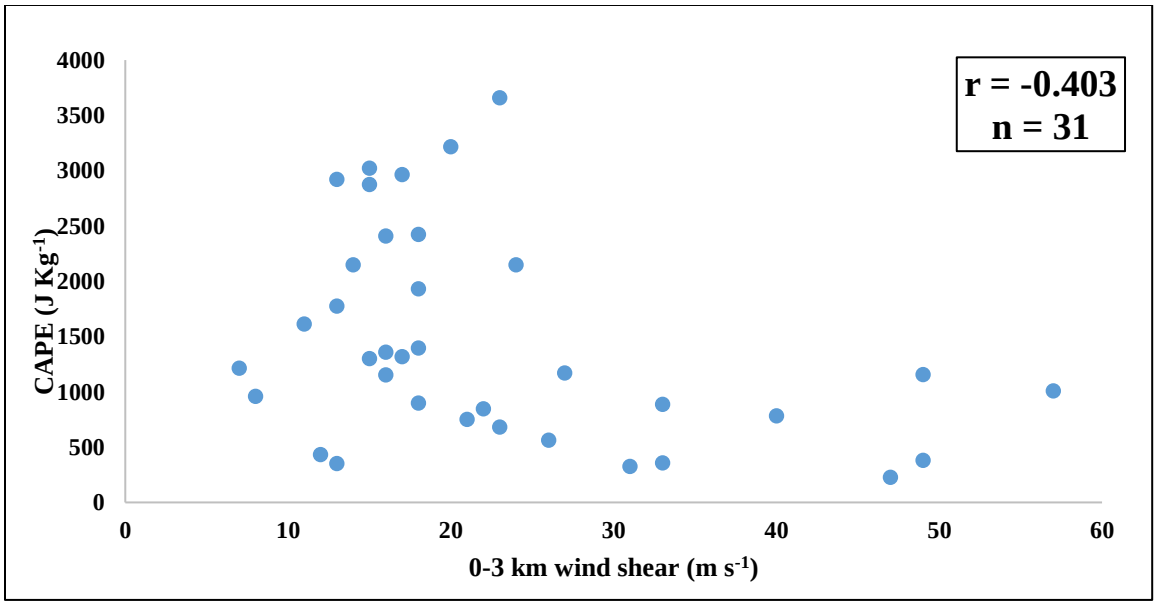

Figure 4.6 Scatterplot for MUCAPE versus 0-3 km wind shear (m s^{-1}).

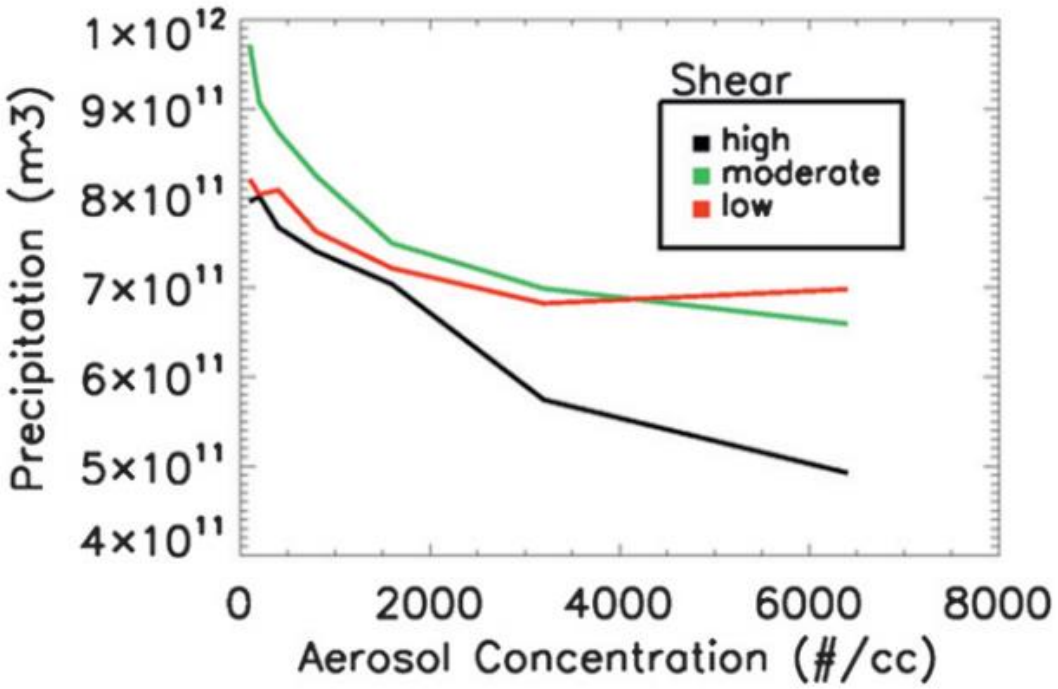

Figure 4.7: Total volumetric precipitation vs. aerosol concentration with high shear = 50 m s^{-1}; moderate shear = 30 m s^{-1} and low shear = 10 m s^{-1} (from Storer et al. (2010) Fig. 11)

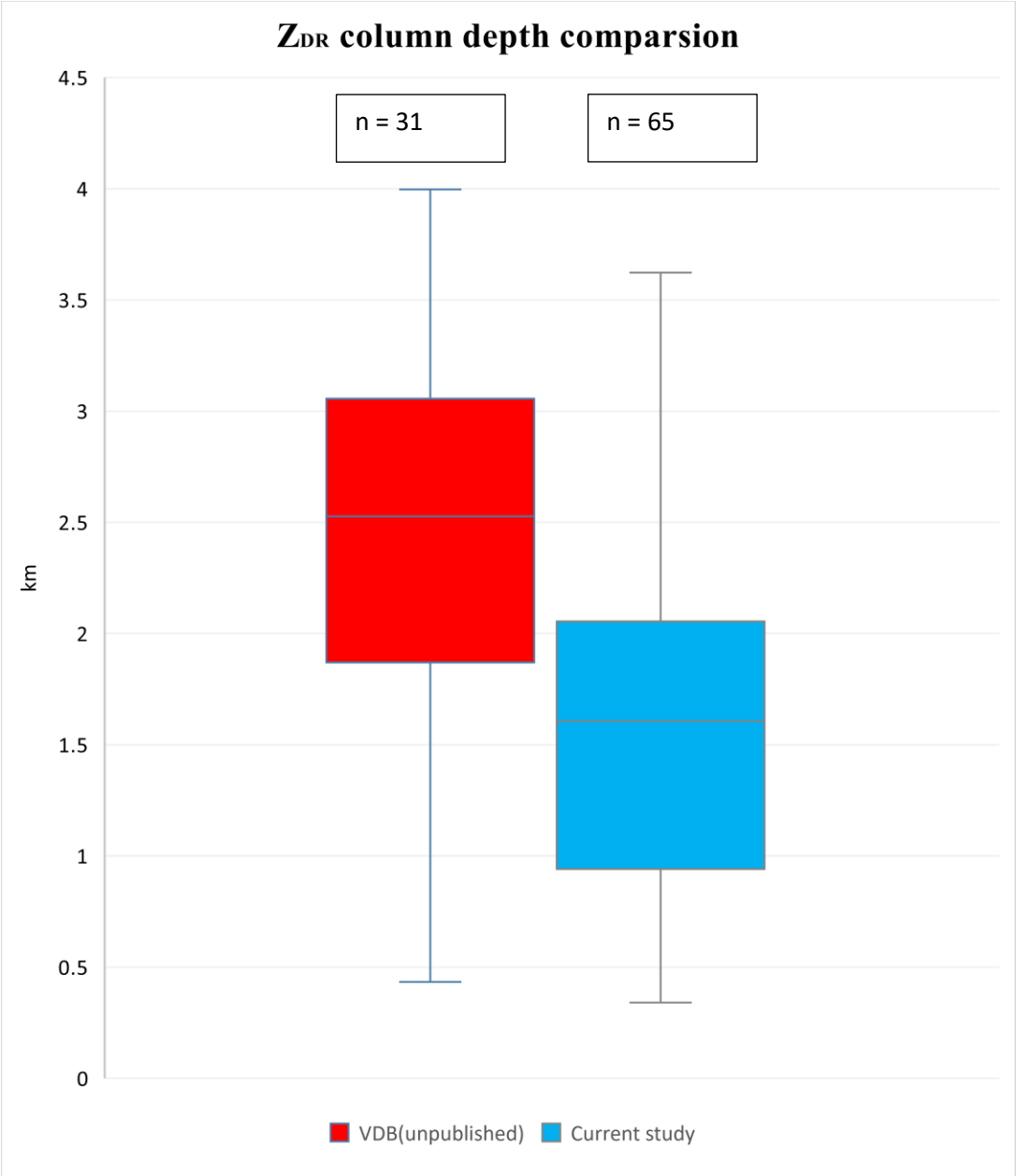

Figure 4.8 Observed Z_{DR} column depth for Van Den Broeke (unpublished) and the current study.

Table 4.1 Pearson's correlation between mean Z_{DR} and several other variables including CCN concentration, freezing level, LCL temperature, 0-3 km shear and MUCAPE (left column). Columns to the right indicate correlation between environmental variables.

	Z_{DR} (dB)	CCN Concentration (cm^{-3})	Freezing level (m)	LCL Temperature (°C)	0-3 km Shear ($m\ s^{-1}$)
CCN Concentration (cm^{-3})	-0.228				
Freezing level (m)	-0.167	0.162			
LCL Temperature (°C)	-0.181	0.191	0.542		
0-3 km Shear ($m\ s^{-1}$)	-0.080	0.104	-0.046	0.093	
MUCAPE ($J\ kg^{-1}$)	0.530	-0.222	-0.242	-0.137	-0.403

5. Z_{DR} Column Characteristics Associated with CCN Concentration and Environmental Variables

The differential reflectivity (Z_{DR}) column represents a comparatively narrow zone of enhanced Z_{DR} as liquid droplets are lofted above the environmental freezing level (e.g., Wakimoto and Bringi 1988; Kumjian et al. 2010). The column is often found in strong convective updrafts with distinct regions of relatively high Z_{DR} compared to their surroundings (e.g., Illingworth et al. 1987; Brandes et al. 1995). The Z_{DR} column can be used to infer updraft characteristics including its strength (e.g., Illingworth et al. 1987; Wakimoto and Bringi 1988; Conway and Zrnić 1993; Brandes et al. 1995; Jameson et al. 1996; Hubbert et al. 1998; Kumjian and Ryzhkov 2008; Snyder et al. 2013; Kumjian et al. 2014; Snyder et al. 2015; Van Den Broeke 2016). The local environmental freezing level is shifted upward as result of vertical advection in moist adiabatic ascent and latent heating within the storm updraft, thus liquid raindrops near the updraft can be lofted beyond the environmental freezing level (Snyder et al. 2015). Since aerosol loading affects storm microphysics (e.g., Rosenfeld 1999, 2000; Andreae et al. 2004; Koren et al. 2005), it is important to understand how the depth of the Z_{DR} column varies as a function of CCN concentration, and how this association is modulated by environmental variables.

The radar dataset used for this analysis consists of 66 storms. Representative values of environmental variables (Table 5.1) were taken from RAP (n = 51)/RUC (n = 15) soundings to characterize each storm-scale environment and examine which variables are more influential on Z_{DR} column depth. These results are compared with those of Van Den Broeke (2016) to understand how updraft characteristics vary in a different set of convective environments−whereas the storms studied by Van Den Broeke (2016) were

supercells, most (98.5%) were nonsupercells in this dataset. Environmental parameters were consistent with those used by Van Den Broeke (2016) to characterize storm-scale environments.

Table 5.1 shows Pearson's correlation between Z_{DR} column depth, CCN concentration, and several other environmental variables which were hypothesized to influence Z_{DR} column depth. There was a positive correlation between Z_{DR} column depth and CCN concentration ($r = 0.624$) and MUCAPE ($r = 0.402$). CCN concentration and MUCAPE are theoretically related to Z_{DR} column depth because larger CCN concentration produces more small droplets and leads to a less efficient collision-coalescence process, resulting in delayed raindrop formation above the freezing level (Rosenfeld 1999; 2000). The 0-6 km shear, which controls the degree of organization and severity of supercell storms, should correlate with Z_{DR} column depth (e.g., Snyder et al. 2015; Van Den Broeke 2016). However, a weak correlation was found ($r = -0.079$). This implies that wind shear is not a major contributing variable for Z_{DR} column depth for this sample of nonsupercell storms, which were associated with relatively weak vertical wind shear. Other environmental variables (freezing level, LCL temperature, LFC temperature; Table 5.1) are also weakly correlated to Z_{DR} column depth. Prior observations and simulations did not find strong evidence to indicate how these environmental parameters may be correlated to Z_{DR} column depth in different CCN concentration regimes.

The distribution of CCN concentration versus Z_{DR} column depth has a positive relationship (Figure 5.1). Simulations by Ilotoviz et al. (2018) found the height of the Z_{DR} column increases with an increase in aerosol concentration (Figure 5.2). In addition, Z_{DR} column depth may also vary depending on the local ambient 0°C level and updraft

intensity (e.g., in the case when vertical velocities are ≥ 30 m s^{-1}, the ambient 0°C level is lifted by a few hundred meters; Ilotoviz et al. 2018). Therefore, the height of the local ambient 0°C level is also affected by the updraft intensity; this could be a limitation of the dataset used in the study since this height was not observed. The distribution of aerosol concentration and Z_{DR} column depth in the cases analyzed here had a strong correlation (r = 0.624), and are generally in agreement with numerical model results by Ilotoviz et al. (2018) who found a correlation between similar variables of 0.88 (Figure 5.5). Ilotoviz et al. (2018) discovered the main difference in characteristics of Z_{DR} columns between high (3000 cm^{-3}) and low (100 cm^{-3}) CCN concentration is a reduced amount of supercooled cloud water content (CWC) in the low-CCN case. The CWC maximum in the low CCN case is located at about half the altitude (CWC ≥ 1 g m^{-3} was reached at 4 km in the clean case and 7 km in the polluted case) and with altered magnitude (~1.3 g m^{-3} in the low CCN case and ~2.75 g m^{-3} in the high CCN case). The Z_{DR} column depth in the polluted case (N_0 = 3000 cm^{-3}) was 1 to 1.5 km greater than in the clean case (N_0 = 100 cm^{-3}). In the low-CCN case, cloud droplets are relatively large compared to the polluted case, and raindrops likely formed near, but below, the freezing level causing some droplets to fall to the ground without reaching the environmental 0°C level (Figure 5.3). This results in a shallower Z_{DR} column compared to the high CCN concentration case.

Previous simulations and observations by Snyder et al. (2015) found that increased CAPE leads to deeper Z_{DR} columns. The presence of a Z_{DR} column indicates a positive temperature perturbation above the freezing level; this can also be used as a measure of the convective updraft intensity (e.g., Kumjian et al. 2010). Since MUCAPE is directly

related to the maximum potential vertical velocity within an updraft, it is hypothesized that there should be a positive relationship between the Z_{DR} column depth and MUCAPE since high MUCAPE should result in stronger vertical acceleration and therefore a larger quantity of droplets lofted above the freezing level. Figure 5.4 shows a positive correlation between the Z_{DR} column depth and MUCAPE ($r = 0.402$), consistent with the theoretical expectation. The nonsupercell convective storms also tend to have weaker updrafts, resulting in shallower Z_{DR} columns. To determine if the difference of updraft intensity between supercell nonsupercell storms is statistically significant, the dataset here, consisting of mostly nonsupercell storms, is compared with supercell storms studied by Van Den Broeke (2016). Z_{DR} column depth is generally deeper in the supercell storms (Table 5.1 and Van Den Broeke (2016): 1.163 km vs. 2.229 km) with a significant difference ($p < 0.01$) in the Wilcoxon-Mann-Whitney (WMW) rank-sum test).

Environmental variables such as MUCAPE and wind shear are known to strongly influence thunderstorm structure, microphysics, and updraft characteristics and provide initial guidance about how storms may vary microphysically between days with different environments. A predictive equation for Z_{DR} column depth was developed using multiple linear regression from a set of predictors including environmental variables and CCN concentration. The environmental variables selected as possible predictors include all the variables in Table 5.1 associated with Z_{DR} columns. Environmental parameters were first checked for collinearity and the stepwise multiple regression as described in chapter 4. The maximum condition index value was 17.76, indicating non-severe collinearity and allowing all variables to be retained within the predictive equation. Then using the stepwise multiple regression to exclude parameters that were not significant ($p \geq 0.05$),

a model developed werer developled that explains 42.1% of the variance in Z_{DR} column depth (km):

$$Z_{DR} \text{ column depth (km)} = 2.67 + 5.52 \times 10^{-4}\,(a) - 6.10 \times 10^{-4}\,(b) + 2.31 \times 10^{-4}\,(c), \quad (4)$$

Where *a* is CCN concentration (cm^{-3}), *b* is the freezing level (m), and *c* is MUCAPE ($J\ Kg^{-1}$). CCN was strongly positively correlated to Z_{DR} column depth (Figure 5.1) likely because high CCN concentration is associated with high supercooled CWC and therefore a deeper Z_{DR} column (Ilotoviz et al. 2018). MUCAPE was moderately correlated to this metric, likely because a strong vertical acceleration is associated with higher MUCAPE, therefore promoting droplets to be lofted above the freezing level resulting in deeper Z_{DR} columns. LFC temperature, ESRH, 0-6 km shear, LCL temperature, and freezing level individually are weakly correlated to this metric. These individual parameters may indirectly contribute to Z_{DR} column depth in combination with other variables even if they are not substantially correlated with Z_{DR} column depth by themselves.

In the previous observational study by Van Den Broeke (2016), Z_{DR} column metrics were analyzed as a function of environmental variability, providing initial guidance about how radar features associated with supercell storms vary between environments. The results show that certain environmental parameters (MUCAPE, ESRH, and LCL temperature) have a moderately strong correlation with mean Z_{DR} column altitude in supercell environments. The dataset in the current study contains mostly (~98%) nonsupercell storms. Nonsupercell convective storms tend to have weaker updraft vertical velocity compared to supercells (Snyder et al. 2015), which was shown to be the case for this

dataset. Supercells also exhibit relatively well-known radar updraft signatures (e.g., bounded weak echo region; Moller et al. 1994; Bunkers et al. 2006); therefore it is hypothesized that environmental parameters will be more weakly correlated to the Z_{DR} column depth for storms included in this study.

A regression (5) explained 75% of the variance in 1-dB Z_{DR} column depth (km) in a sample of supercell storms by Van Den Broeke (2016):

$$Z_{DR} \text{ column altitude above } 0°C \text{ level (km)}$$

$$= 0.96 + 3.85 \times 10^{-4} (a) + 2.49 \times 10^{-3} (b) - 1.2 \times 10^{-2} (c), \quad (5)$$

Where a is MUCAPE (J Kg^{-1}), b is ESRH (m^2 s^{-2}), and c is the LCL temperature (°C). This predictive equation was applied to the set of nonsupercell storms in this study to see whether it still has value for nonsupercell storms. The observed Z_{DR} column depth in the nonsupercell storms is generally shallower compared to the value predicted by (5) (Figure 5.6). This is consistent with the theoretical expectations since this equation was derived specifically for supercell environments. ESRH might affect the result if most observed thunderstorms were surface-base as the ESRH yield more substantial results for SRH in elevated thunderstorms (Thompson et al. 2007).

Another comparison for Z_{DR} column depth was done using observed non-tornadic supercell storms (n = 31) from Van Den Broeke (personal communication, 2018) and observed nonsupercell storms in this dataset (n = 65). There was a significant difference ($p < 0.01$) of average Z_{DR} column depth between observed non-tornadic supercell storms and observed thunderstorms in nonsupercell environments in this dataset. The 0-6 km shear has a very low correlation to Z_{DR} column depth in this study (r = -0.079). The Z_{DR}

column depth for the non-tornadic storms in supercell environments is generally larger compared to those in nonsupercell environments in the current study (Figure 4.8).

Table 5.1 Pearson's correlation between Z_{DR} column depth and several environmental variables including CCN concentration, LCL temperature, ESRH, MUCAPE, LFC temperature and 0-6 km shear (first column of values). Columns to the right indicate correlation between environmental variables.

	Z_{DR} Column Depth (m)	CCN Concentration (cm^{-3})	LCL Temperature (°C)	ESRH ($m^2\ s^{-2}$)	MUCAPE ($J\ kg^{-1}$)	LFC Temperature (°C)	0-6 km Shear ($m\ s^{-1}$)
CCN Concentration (cm^{-3})	0.624						
LCL Temperature (°C)	0.092	0.182					
ESRH ($m^2\ s^{-2}$)	-0.007	-0.135	0.154				
MUCAPE ($J\ kg^{-1}$)	0.402	0.268	0.206	0.005			
LFC Temperature (°C)	0.036	-0.047	0.091	0.033	0.311		
0-6 km Shear ($m\ s^{-1}$)	-0.079	-0.070	0.267	0.432	-0.077	-0.274	
Freezing Level (m)	-0.008	0.403	0.298	-0.056	0.120	-0.054	-0.167

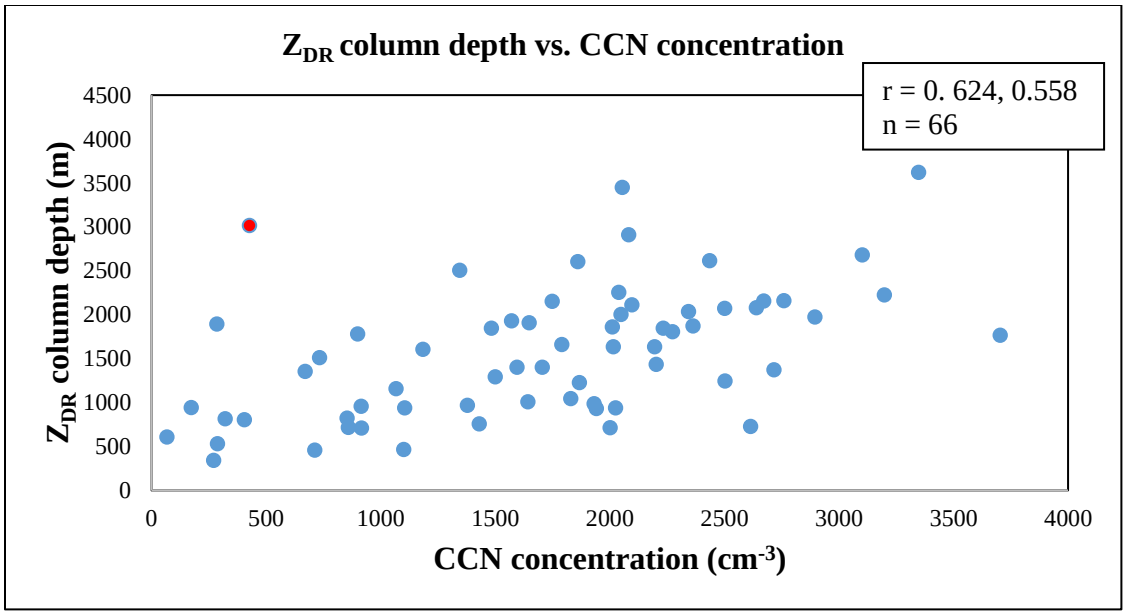

Figure 5.1 Scatterplot of mean Z_{DR} column depth (m) versus CCN concentration (cm^{-3}). Each dot represents one storm. Red dot indicates outlier (supercell), the first r value corresponds to outlier removed and the second corresponds to all points included.

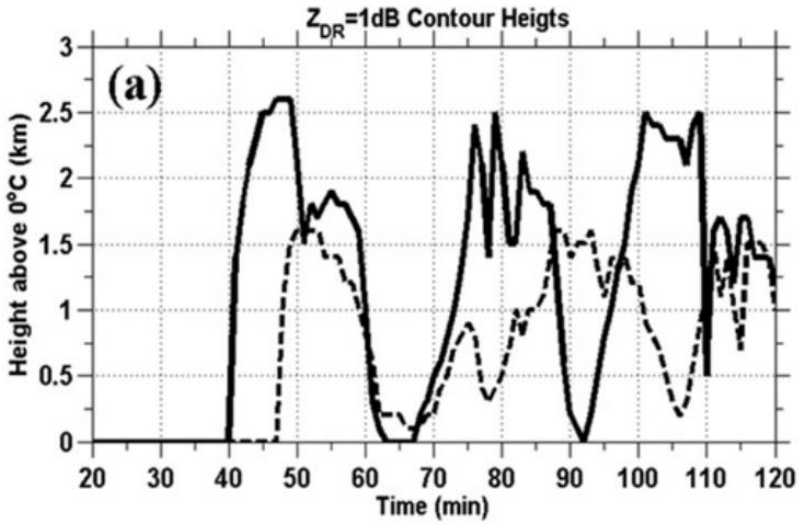

Figure 5.2: Z_{DR} column height at high CCN concentration (solid line) and low concentration (dashed line) (from Ilotoviz et al. (2018), Fig. 17a).

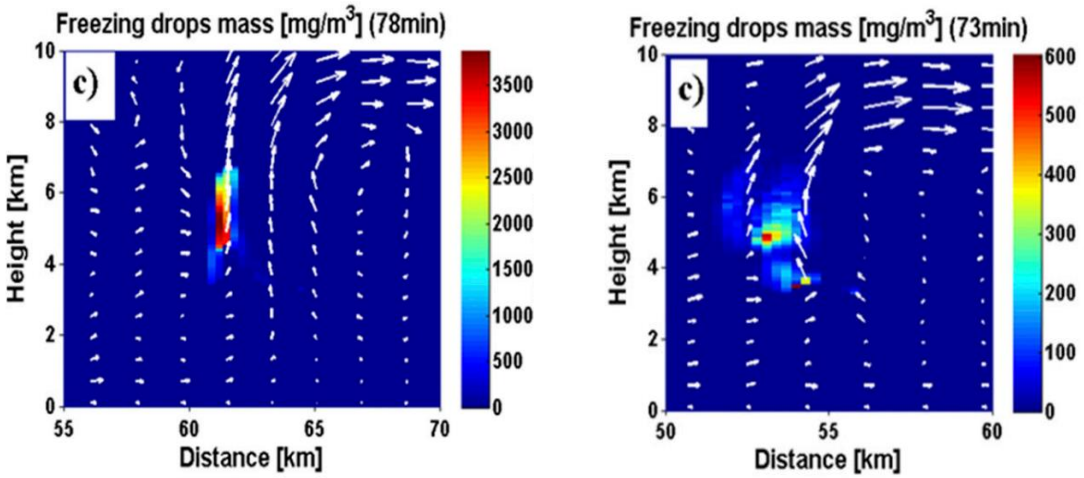

Figure 5.3: Freezing drop mass under high CCN concentration (left) and low CCN concentration (right) (from Ilotoviz et al. (2018), Figs. 8c and 14c).

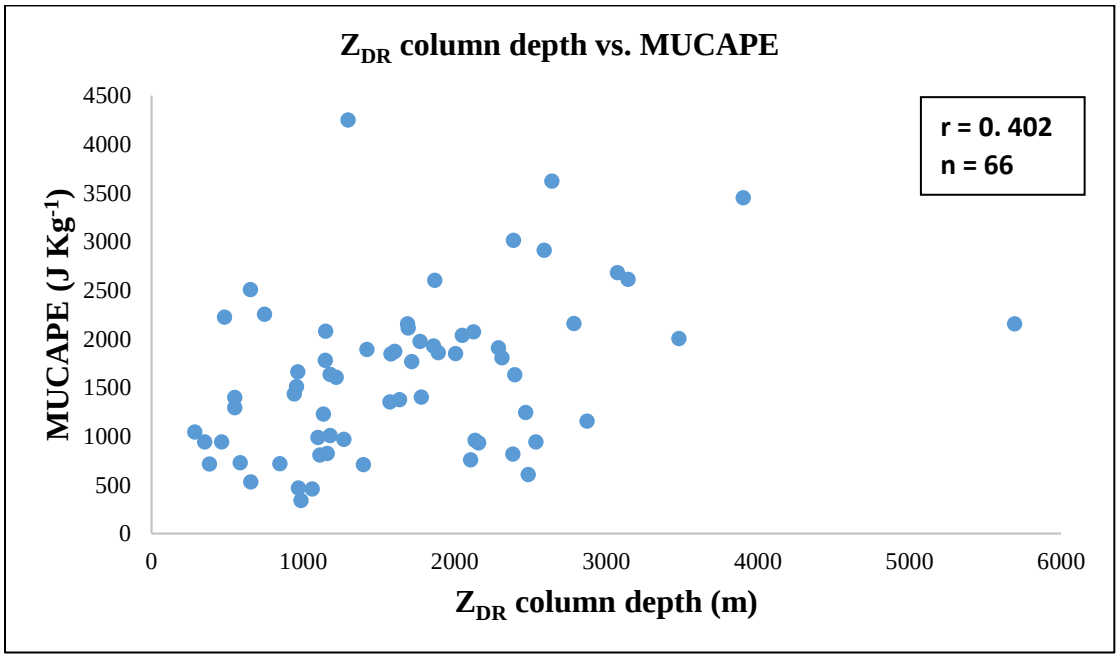

Figure 5.4 Scatterplot of Z_{DR} column depth (m) versus MUCAPE (J Kg^{-1}).

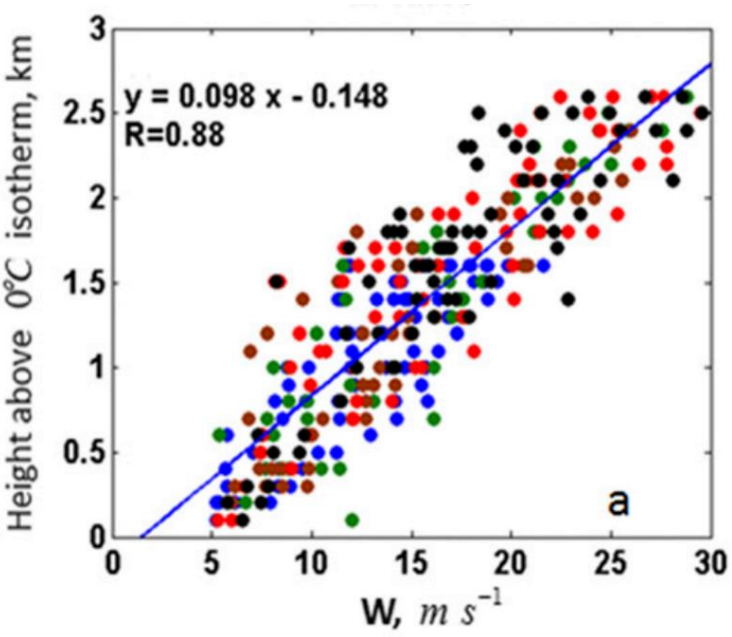

Figure 5.5: Scatterplot of height of Z_{DR} = 1 dB vs. vertical velocity for different CCN concentration (blue: 100 cm^{-3}; green: 400 cm^{-3}; brown: 1000 cm^{-3}; red: 2000 cm^{-3}; and black: 3000 cm^{-3}) from Ilotoviz et al. (2018), Fig. 19a.

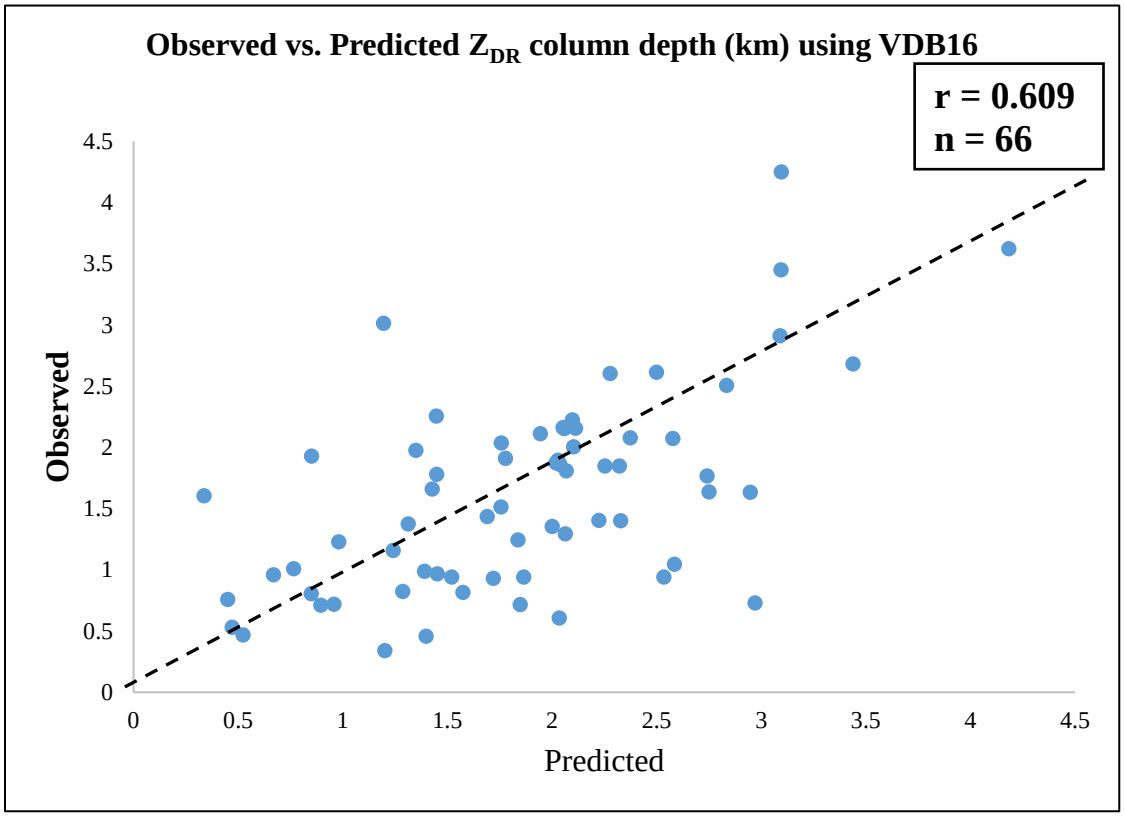
Observed vs. Predicted Z_{DR} column depth (km) using VDB16
r = 0.609
n = 66
Observed
Predicted
0
0.5
1
1.5
2
2.5
3
3.5
4
4.5

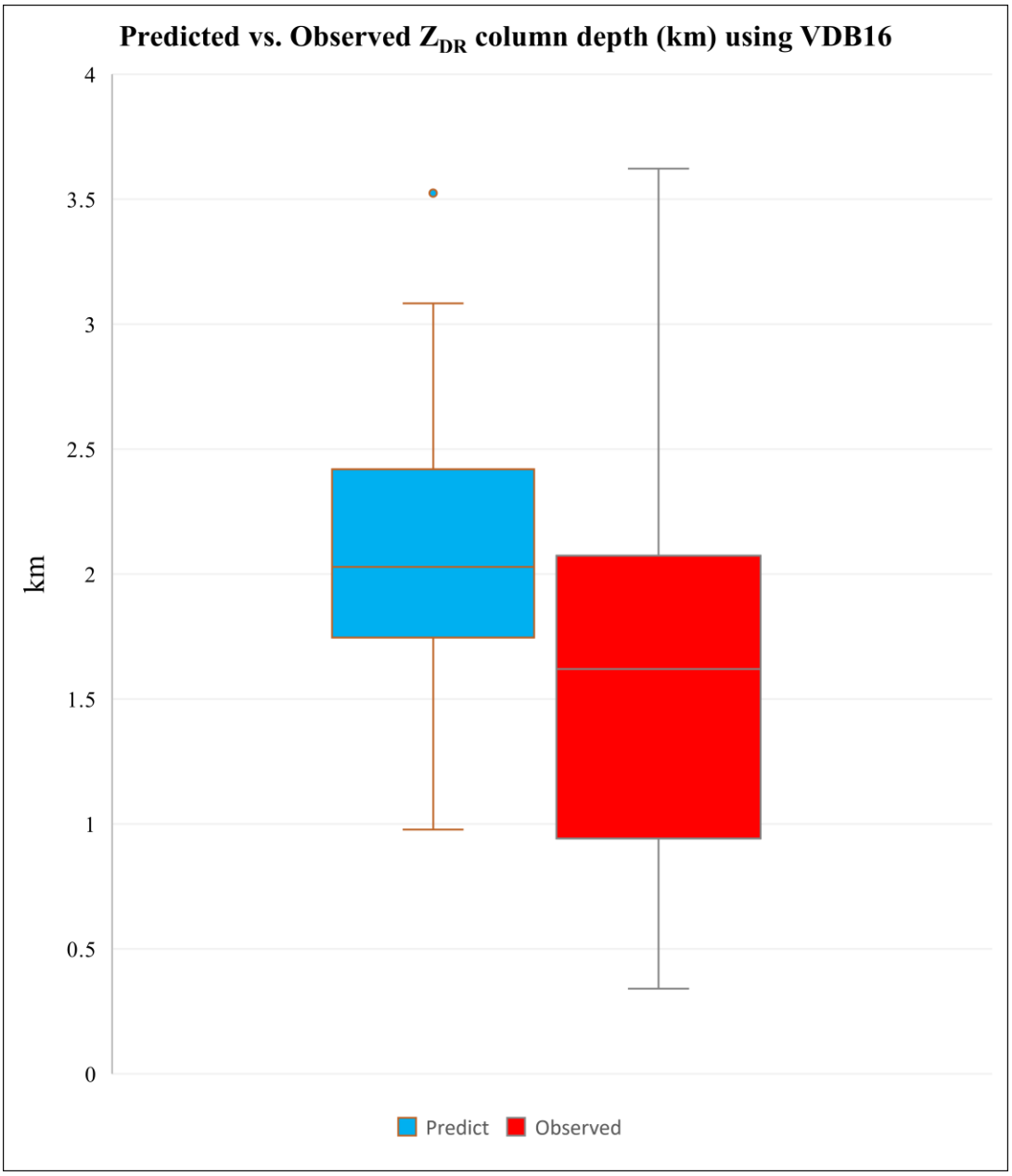

Figure 5.6: Predicted vs. Observed Z_{DR} column depth (km) of 66 storms using VDB16 equation (1). Scatter plot for observed vs. predicted (above).

6. Discussion and Conclusions

Storm microphysics and associated radar characteristics can be impacted by CCN concentration and other environmental parameters. The preliminary observational results in this study highlight the importance of CCN concentration and the storm-scale environment on storm microphysical structure (e.g., mean droplet size, Z_{DR} column depth). These effects were assessed using a dataset composed of 36 thunderstorms for mean droplet size within 75 km of a WSR-88D and 66 thunderstorms for Z_{DR} column depth within 100 km of a WSR-88D across a wide range of environments. This study provides additional observational evidence of how CCN concentration and associated environmental variability affects the mean droplet sizes and the Z_{DR} column depth in continental thunderstorms.

A moderate correlation was found between mean Z_{DR} (closely related to mean drop size in a sample volume) and CCN concentration ($r = -0.228$) within 20 min of convection initiation, with stronger correlation ($r = -0.365$) associated with higher radar reflectivity values. These high reflectivity regions indicate the approximate location of strong updraft. Stronger vertical acceleration promotes size sorting, and thus the trends of droplet-size characteristics as a function of aerosol concentration are more apparent. MUCAPE was also strongly associated with droplet size as stronger updraft enhances the collision-coalescence process. Other environmental parameters (e.g., the freezing altitude, LCL temperature, and 0-3 km shear) were weakly associated with mean droplet size in convective updrafts. A predictive equation for mean Z_{DR} value was developed using multiple linear regression and a combination of predictor variables including CCN

concentration, shear and instability parameters. Environmental parameters were checked for collinearity to ensure the parameters contained sufficiently unique information, following by the stepwise multiple regression to eliminate the variable that is not significant ($p > 0.05$) and the resulting predictive equation explained 29.5% of the variability in mean Z_{DR} (dB).

Aerosol concentration was strongly correlated with Z_{DR} column depth. This result supports previous research (e.g., Ilotoviz et al. 2018) that an increase in CCN concentration is associated with larger Z_{DR} columns and stronger updraft. Since high CCN concentration is associated with high supercooled CWC resulting in a deeper Z_{DR} column, CCN concentration was strongly positively correlated to Z_{DR} column depth. Additionally, MUCAPE was positively correlated to Z_{DR} column depth, providing additional observational evidence of strong updraft in high-MUCAPE environments. A predictive equation was developed for Z_{DR} column depth using linear regression. It used CCN concentration and environmental parameters with theoretically supporting evidence of a link to updraft strength, and explained 42.1% of the variability in Z_{DR} column depth. Individual parameters (e.g., LFC temperature, ESRH, and 0-6 km shear), though weakly correlated to this metric, may indirectly contribute to Z_{DR} column depth in combination with other variables even if they were not significantly correlated with Z_{DR} column depth by themselves.

A predictive equation developed by Van Den Broeke (2016) was used to examine differences of Z_{DR} column depth predictability between supercell and nonsupercell storms. Observed Z_{DR} column depth was shallower among the nonsupercell storms compared to the predicted values using an equation developed for supercell storms. The

predictability is higher for the supercell environment than for nonsupercells. This was likely a result of equation from Van Den Broeke (2016) is explicitly developed for supercell environments. The supercell environment also supports deeper Z_{DR} columns (e.g., vertical wind shear, high MUCAPE). The dataset in this project included a large variety of primarily nonsupercell thunderstorm modes; therefore, certain conditions may not be fully captured by the environmental parameters.

Significant differences of Z_{DR} column depth were found between non-tornadic storms in supercell environments from Van Den Broeke (unpublished; n = 31) and non-tornadic nonsupercell environments in this study (n = 65). The mean Z_{DR} column depth in non-tornadic storms in the supercell environment is ~0.9 km larger compared to storms in nonsupercell environments (($p < 0.01$). Z_{DR} column depth was strongly correlated with MUCAPE and ESRH. LCL temperature was not strongly correlated to Z_{DR} column depth in this dataset (r = 0.092). Van Den Broeke (2016), however, showed that LCL temperature is positively associated with Z_{DR} column depth (r = 0.61 in that study). The depth of Z_{DR} columns is influenced by LCL temperature as warm LCL temperatures may imply more cloud at warmer conditions and therefore a potential to be associated with higher-altitude Z_{DR} columns (Van Den Broeke 2016).

Results of this study support that the CCN effect and MUCAPE are more influential among this set of storms relative to the effects of other environmental variability as an increase in CCN concentration was associated with smaller mean droplet size shortly after storm initiation. However, higher MUCAPE was more influential for the mean drop size. In addition, the higher reflectivity region was associated with a more negative correlation with mean drop size, providing additional observational evidence that CCN

concentration influences mean drop size especially in the region of the strongest updraft. There is also evidence that increasing MUCAPE was associated with larger droplet size, which supports previous modeling studies (e.g., Lee et al. 2008). A possible explanation for this result is that the strong updraft in a high MUCAPE environment enhances the collision-coalescence process at low levels, resulting in larger droplets. Previous studies also suggest that the height of the freezing level may determine the relative importance of the warm-rain process during the early stage of a storm. This could affect the aerosol loading and alter the cloud microphysics (e.g., Fan et al. 2012) as the distance varies between the cloud base and freezing level for coalescence into raindrops. For example, if the distance between the cloud base and freezing level is small, the CCN concentration has less potential to influence the rain process. However, it did not show a significant correlation in this research.

Results from this sample of storms show evidence of a strong CCN concentration influence on storm microphysical structure in the early and mid-stage of convection. When comparing CCN across different environments, there is a negative correlation associated with mean Z_{DR} and positive correlation with Z_{DR} column depth, indicating that CCN concentration can alter the storm microphysics. MUCAPE increased with increasing mean Z_{DR}; this was similar to Z_{DR} column depth but less pronounced. When all environmental parameters were considered, CCN and MUCAPE were the most significant factors (respectively, -0.365, 0.530 for mean Z_{DR}; 0.624, 0.402 for Z_{DR} column depth). The results herein underscore the complex interactions between storm microphysics and different environmental parameters. They show a higher sensitivity of Z_{DR} column depth to CCN concentration than to other environmental variability.

Therefore, future work may include adding CCN to the dataset used to predict polarimetric characteristics of thunderstorms (Z_{DR} column areal extent, Z_{DR} arc and Z_{DR} column depth) to continue to understand how CCN concentration may alter storm microphysics under various environments and whether it is necessary to include this variable into an assessment of radar-derived fields. It is important to remember that some environmental parameters are not feasible to estimate. Additionally, there might be many factors not described by the environmental variables in this study that affect microphysical processes.

7. References

Alberoni, P. P., V. Levizzani, R. J. Watson, A. R. Holt, S. Costa, P. Mezzasalma, and S. Nanni, 2000: The 18 June 1997 companion supercells: Multiparametric Doppler radar analysis. *Meteorol. Atmos. Phys.*, **75**, 101–120, doi:10.1007/s007030070018.

Altaratz, O., I. Koren, L. A. Remer, and E. Hirsch, 2014: Review: Cloud invigoration by aerosols-coupling between microphysics and dynamics. *Atmos. Res.*, **140**–**141**, 38–60, doi:10.1016/j.atmosres.2014.01.009.

Andreae, M. O., D. Rosenfeld, P. Artaxo, A. A. Costa, G. P. Frank, K. M. Longo, and M. A. F. Silva-Dias, 2004: Smoking rain clouds over the amazon. *Science*, **303**, 1337–1342, doi:10.1126/science.1092779.

Andreae, M. O., 2009: Correlation between cloud condensation nuclei concentration and aerosol optical thickness in remote and polluted regions. *Atmos. Chem. Phys.*, **9**, 543–556, doi:10.5194/acp-9-543-2009.

Bechini, R., L. Baldini, R. Cremonini, and E. Gorgucci, 2008: Differential reflectivity calibration for operational radars. *J. Atmos. Ocean. Technol.*, **25**, 1542–1555, doi:10.1175/2008JTECHA1037.1.

Bell, T. L., D. Rosenfeld, K. M. Kim, J. M. Yoo, M. I. Lee, and M. Hahnenberger, 2008: Midweek increase in U.S. summer rain and storm heights suggests air pollution invigorates rainstorms. *J. Geophys. Res. Atmos.*, **113**, D02209, doi:10.1029/2007JD008623.

Bell, T. L., D. Rosenfeld, and K. M. Kim, 2009: Weekly cycle of lightning: Evidence of storm invigoration by pollution. *Geophys. Res. Lett.*, **36**, L23805, doi:10.1029/2009GL040915.

Belsley, D. a., E. Kuh, and R. E. Welsch, 2005: Regression diagnostics: Identifying influential data and sources of collinearity. *Regression Diagnostic: Identifying influential data and sources of collinearity*, p. 292.

Benjamin, S. G., J. M. Brown, and T. G. Smirnova, 2016: Explicit precipitation-type diagnosis from a model using a mixed-phase bulk cloud–Precipitation microphysics parameterization. *Wea. Forecasting*, **31**, 609–619, doi:10.1175/WAF-D-15-0136.1.

Benjamin, S. G., and Coauthors, 2016: A North American hourly assimilation and model forecast cycle: The Rapid Refresh. *Mon. Wea. Rev.*, **144**, 1669–1694, doi:10.1175/MWR-D-15-0242.1.

Blanchard, D. C., and A. H. Woodcock, 1980: The production, concentration, and vertical distribution of the sea-salt aerosol. *Ann. N. Y. Acad. Sci.*, **338**, 330–347, doi:10.1111/j.1749-6632.1980.tb17130.x.

Brandes, E. A., J. Vivekanandan, J. D. Tuttle, and C. J. Kessinger, 1995: A study of thunderstorm microphysics with multiparameter radar and aircraft observations. *Mon. Wea. Rev.*, **123**, 3129–3143, doi:10.1175/1520-0493(1995)123<3129:ASOTMW>2.0.CO;2.

Bringi, V. N., V. Chandrasekar, and R. Xiao, 1998: Raindrop axis ratio and size distributions in Florida rainshafts: An assessment of multiparameter radar algorithms. *IEEE Trans. Geosci. Remote Sens*, **36,** 703–715.

Bunkers, M. J., M. R. Hjelmfelt, and P. L. Smith, 2006: An observational examination of long-lived supercells. Part I: Characteristics, evolution, and demise. *Wea. Forecasting*, **21**, 673–688, doi:10.1175/WAF949.1.

Clavner, M., W. R. Cotton, S. C. van den Heever, S. M. Saleeby, and J. R. Pierce, 2018: The response of a simulated mesoscale convective system to increased aerosol pollution: Part I: Precipitation intensity, distribution, and efficiency. *Atmos. Res.*, **199**, 193–208, doi:10.1016/j.atmosres.2017.08.010.

Chou, C., J. D. Neelin, U. Lohmann, and J. Feichter, 2005: Local and remote impacts of aerosol climate forcing on tropical precipitation. *J. Climate*, **18,** 4621–4636.

Conway, J. W., and D. S. Zrnić, 1993: A study of embryo production and hail growth using dual-doppler and multiparameter radars. *Mon. Wea. Rev.*, **121**, 2511–2528, doi:10.1175/1520-0493(1993)121<2511:ASOEPA>2.0.CO;2.

Dagan, G., I. Koren, and O. Altaratz, 2015: Competition between core and periphery-based processes in warm convective clouds - from invigoration to suppression. *Atmos. Chem. Phys.*, **15**, 2749–2760, doi:10.5194/acp-15-2749-2015.

Devenish, B. J., K. Furtado, and D. J. Thomson, 2016: Analytical solutions of the supersaturation equation for a warm cloud. *J. Atmos. Sci.*, **73**, 3453–3465, doi:10.1175/JAS-D-15-0281.1.

Department of Energy. (2018). *ARM*. Retrieved from Instruments CCN Data: https://www.arm.gov/data

U.S. Department of Energy Office of Science. (2018, May). Retrieved from CCN: Cloud Condensation Nuclei Particle Counter: https://www.arm.gov/capabilities/instruments/ccn

Department of Energy. (2018). *ARM*. Retrieved from Instruments CCN Data: https://www.arm.gov/data

Department of Energy.,Accessed 2019, February 22 2018, *Pacific Northwest National Laboratory*. Retrieved from Aerosol Climate Initiative: https://www.pnnl.gov/atmospheric/research/aci/aci_aerosol_indeffects.stm

U.S. Department of Energy Office of Science. (2018, May). Retrieved from CCN: Cloud Condensation Nuclei Particle Counter: https://www.arm.gov/capabilities/instruments/ccn

Doviak and D. S. Zrnić, 2006: Doppler Radar and Weather Observations. 2nd ed. Dover Publications, 562 pp.

Fan, J., R. Zhang, G. Li, and W. K. Tao, 2007: Effects of aerosols and relative humidity on cumulus clouds. *J. Geophys. Res. Atmos.*, **112**, D14204, doi:10.1029/2006JD008136.

Fan, J., and Coauthors, 2009: Dominant role by vertical wind shear in regulating aerosol effects on deep convective clouds. *J. Geophys. Res. Atmos.*, **114**, D012352, doi:10.1029/2009JD012352.

Fan, J., L. R. Leung, Z. Li, H. Morrison, H. Chen, Y. Zhou, Y. Qian, and Y. Wang, 2012: Aerosol impacts on clouds and precipitation in eastern China: Results from bin and bulk microphysics. *J. Geophys. Res. Atmos.*, **117**, doi:10.1029/2011JD016537.

Fan, J., L. R. Leung, D. Rosenfeld, Q. Chen, Z. Li, J. Zhang, and H. Yan, 2013: Microphysical effects determine macrophysical response for aerosol impacts on deep convective clouds. *Proc. Natl. Acad. Sci.*, **110**, E4581–E4590, doi:10.1073/pnas.1316830110.

Ghan, S. (2018, July). *Pacific Northwest National Laboratory*. Retrieved from Aerosol Indirect Effects: https://www.pnnl.gov/atmospheric/research/aci/aci_aerosol_indeffects.stm

Goudenhoofdt, E., and L. Delobbe, 2013: Statistical characteristics of convective storms in belgium derived from volumetric weather radar observations. *J. Appl. Meteor. Clim.*, **52**, 918–934, doi:10.1175/JAMC-D-12-079.1.

Gorgucci, E., G. Scarchilli, and V. Chandrasekar, 1992: Calibration of radars using polarimetric techniques. *IEEE Trans. Geosci. Remote Sens.*, **30**, 853–858, doi:10.1109/36.175319.

Hubbert, J., V. N. Bringi, L. D. Carey, and S. Bolen, 1998: CSU-CHILL polarimetric radar measurements from a severe hail storm in eastern Colorado. *J. Appl. Meteor.*, **37**, 749–775, doi:10.1175/1520-0450(1998)037<0749:CCPRMF>2.0.CO;2.

Illingworth, A. J., J. W. F. Goddard, and S. M. Cherry, 1987: Polarization radar studies of precipitation development in convective storms. *Quart. J. Roy. Meteor. Soc.*, **113**, 469–489, doi:10.1002/qj.49711347604.

Ilotoviz, E., A. P. Khain, N. Benmoshe, V. T. J. Phillips, and A. V. Ryzhkov, 2015: Effect of aerosols on freezing drops, hail, and precipitation in a midlatitude storm. *J. Atmos. Sci.*, **73**, 109–144, doi:10.1175/JAS-D-14-0155.1.

Ilotoviz, E., A. Khain, A. V. Ryzhkov, and J. C. Snyder, 2018: Relationship between aerosols, hail microphysics and Z_{DR} columns. *J. Atmos. Sci.*, **75**, 1755–1781, doi:10.1175/JAS-D-17-0127.1.

Jameson, A. R., M. J. Murphy, and E. P. Krider, 1996: Multi-parameter radar observations of isolated Florida thunderstorms during the onset of electrification. *J. Appl. Meteor.*, **35**, 343–354, doi:10.1207/S15327078IN0302_5.

Kalina, E. A., K. Friedrich, H. Morrison, and G. H. Bryan, 2014: Aerosol effects on idealized supercell thunderstorms in different environments. *J. Atmos. Sci.*, **71**, 4558–4580, doi:10.1175/JAS-D-14-0037.1.

Khain, A., D. Rosenfeld, and A. Pokrovsky, 2005: Aerosol impact on the dynamics and microphysics of deep convective clouds. *Quart. J. Roy. Meteor. Soc.*, **131**, 2639–2663, doi:10.1256/qj.04.62.

Köhler, H., 1936: The nucleus in and the growth of hygroscopic droplets. *Trans. Faraday Soc.*, **32**, 1152–1161, doi:10.1039/TF9363201152.

Koren, I., Y. J. Kaufman, D. Rosenfeld, L. A. Remer, and Y. Rudich, 2005: Aerosol invigoration and restructuring of Atlantic convective clouds. *Geophys. Res. Lett.*, **32**, L14828, doi:10.1029/2005GL023187.

Kumjian, M. R., and A. V. Ryzhkov, 2008: Polarimetric signatures in supercell thunderstorms. *J. Appl. Meteor. Clim.*, **47**, 1940–1961, doi:10.1175/2007JAMC1874.1.

Kumjian, M. R., A. V. Ryzhkov, V. M. Melnikov, and T. J. Schuur, 2010: Rapid-scan super-resolution observations of a cyclic supercell with a dual-polarization WSR-88D. *Mon. Wea. Rev.*, **138**, 3762–3786, doi:10.1175/2010MWR3322.1.

Kumjian, M. R., 2013: Principles and applications of dual-polarization weather radar. Part I: Description of the polarimetric radar variables. *J. Oper. Meteorol.*, **1**, 226–242, doi:10.15191/nwajom.2013.0119.

Kumjian, M. R., A. P. Khain, N. Benmoshe, E. Ilotoviz, A. V. Ryzhkov, and V. T. J. Phillips, 2014: The anatomy and physics of Z_{DR} columns: Investigating a polarimetric radar signature with a spectral bin microphysical model. *J. Appl. Meteor. Clim.*, **53**, 1820–1843, doi:10.1175/JAMC-D-13-0354.1.

Lebo, Z., 2018: A numerical investigation of the potential effects of aerosol-induced warming and updraft Width and slope on updraft intensity in deep convective clouds. *J.*

Atmos. Sci., **75**, 535–554, doi:10.1175/JAS-D-16-0368.1. http://journals.ametsoc.org/doi/10.1175/JAS-D-16-0368.1.

Lee, S. S., L. J. Donner, V. T. J. Phillips, and Y. Ming, 2008: The dependence of aerosol effect on clouds and precipitation on cloud-system organization, shear and stability. *J. Geophys. Res. Atmos.*, **113**, D16202, doi:10.1029/2007JD009224.

Lee, S. S., 2011: Dependence of aerosol-precipitation interactions on humidity in a multiple-cloud system. *Atmos. Chem. Phys.*, **11**, 2179–2196, doi:10.5194/acp-11-2179-2011.

Lerach, D. G., B. J. Gaudet, and W. R. Cotton, 2008: Idealized simulations of aerosol influences on tornadogenesis. *Geophys. Res. Lett.*, **35**, L23806, doi:10.1029/2008GL035617.

Lerach, D. G., and W. R. Cotton, 2012: Comparing aerosol and low-level moisture influences on supercell tornadogenesis: Three-dimensional idealized simulations. *J. Atmos. Sci.*, **69**, 969–987, doi:10.1175/JAS-D-11-043.1.

Li, Z., F. Niu, J. Fan, Y. Liu, D. Rosenfeld, and Y. Ding, 2011: Long-term impacts of aerosols on the vertical development of clouds and precipitation. *Nat. Geosci.*, **4**, 888–894, doi:10.1038/ngeo1313.

Lohmann, U., and G. Lesins, 2003: Comparing continental and oceanic cloud susceptibilities to aerosols. *Geophys. Res. Lett.*, **30**, 1–4, doi:10.1029/2003GL017828.

Lunkenheimer, P., S. Emmert, R. Gulich, M. Köhler, M. Wolf, M. Schwab, and A. Loidl, 2017: Electromagnetic-radiation absorption by water. *Phys. Rev. E*, **96**, doi:10.1103/PhysRevE.96.062607.

Martins, J. V., and Coauthors, 2011: Remote sensing the vertical profile of cloud droplet effective radius, thermodynamic phase, and temperature. *Atmos. Chem. Phys.*, **11**, 9485–9501, doi:10.5194/acp-11-9485-2011.

May, P. T., G. Allen, G. Vaughan, and P. Connolly, 2009: Aerosol and thermodynamic effects on tropical cloud systems during TWPICE and ACTIVE. *Atmos. Chem. Phys.*, **9**, 15–24, doi:10.5194/acp-9-15-2009.

May, P. T., V. N. Bringi, and M. Thurai, 2011: Do we observe aerosol impacts on DSDs in strongly forced tropical thunderstorms? *J. Atmos. Sci.*, **68**, 1902–1910, doi:10.1175/2011JAS3617.1.

Miller, P. W., and T. L. Mote, 2017: A climatology of weakly forced and pulse thunderstorms in the southeast United States. *J. Appl. Meteor. Clim.*, **56**, 3017–3033, doi:10.1175/JAMC-D-17-0005.1.

National Weather Service. (n.d.). Retrieved from Lifting Condensation Level: Retrieved from https://www.weather.gov/btv/profileLCL

NOAA (2018). *National Weather Service*. Supercell Thunderstorm Structure and Evolution. Retrieved from https://www.weather.gov/media/lmk/soo/Supercell_Structure.pdfNOAA National

Severe Storms Laboratory, 2018: *NSSL The National Severe Storms Laboratory*. Retrieved from Severe Weather 101 - Thunderstorms: https://www.nssl.noaa.gov/education/svrwx101/thunderstorms/types/

Picca, J., and A. Ryzhkov, 2012: A dual-wavelength polarimetric analysis of the 16 May 2010 Oklahoma City extreme hailstorm. *Mon. Wea. Rev.*, **140**, 1385–1403, doi:10.1175/MWR-D-11-00112.1.

Plummer, D. M., and Coauthors, 2018: Radar-Derived Structural and Precipitation Characteristics of ZDR Columns within Warm-Season Convection over the United Kingdom. *J. Appl. Meteor. Clim.*, **57**, 2485–2505, doi:10.1175/JAMC-D-17-0134.1.

Potvin, C. K., K. L. Elmore, and S. J. Weiss, 2010: Assessing the impacts of proximity sounding criteria on the climatology of significant tornado environments. *Wea Forecasting.*, **25**, 921–930, doi:10.1175/2010WAF2222368.1.

Pruppacher, H. R., and J. D. Klett, 1997: Equilibrium between water vapour, water, aqueous solutions and ice in bulk. *Microphysics of Clouds and Precipitation*, p. 954.

Rosenfeld, D., and I. M. Lensky, 1998: Satellite-based insights into precipitation formation processes in continental and maritime convective clouds. *Bull. Amer. Meteor. Soc.*, **79**, 2457–2476, doi:10.1175/1520-0477(1998)079<2457:SBIIPF>2.0.CO;2.

Rosenfeld, D., 1999: TRMM observed first direct evidence of smoke from forest fires inhibiting rainfall. *Geophys. Res. Lett.*, **26**, 3105–3108, doi:10.1029/1999GL006066.

Rosenfeld, D., and W. L. Woodley, 2000: Deep convective clouds with sustained supercooled liquid water down to - 37.5 °C. *Nature*, **405**, 440–442, doi:10.1038/35013030.

Rosenfeld, D., and C. W. Ulbrich, 2003: Cloud microphysical properties, processes, and rainfall estimation opportunities. *Meteorol. Monogr.*, **52**, 237–258, doi:10.1175/0065-9401(2003)030<0237:CMPPAR>2.0.CO;2.

Rosenfeld, D., U. Lohmann, G. B. Raga, C. D. O'Dowd, M. Kulmala, S. Fuzzi, A. Reissell, and M. O. Andreae, 2008: Flood or drought: How do aerosols affect precipitation? *Science*, **321**, 1309–1313, doi:10.1126/science.1160606.

Rosenfeld, D., and T. L. Bell, 2011: Why do tornados and hailstorms rest on weekends? *J. Geophys. Res*, **116**, D20211, doi:10.1029/2011JD016214.

Rogers, R. R., and Yau, M. K., 1989: A short course in cloud physics. *Droplet growth by collision and coalescence*, p.132.

Seifert, A., and K. D. Beheng, 2006: A two-moment cloud microphysics parameterization for mixed-phase clouds. Part 1: Model description. *Meteorol. Atmos. Phys.*, **92**, 45–66, doi:10.1007/s00703-005-0112-4.

Snyder, J. C., H. B. Bluestein, V. Venkatesh, and S. J. Frasier, 2013: Observations of polarimetric signatures in supercells by an X-band mobile Doppler radar. *Mon. Wea. Rev.*, **141**, 3–29, doi:10.1175/MWR-D-12-00068.1.

Snyder, J. C., A. V. Ryzhkov, M. R. Kumjian, A. P. Khain, and J. Picca, 2015: A ZDR column detection algorithm to examine convective storm updrafts. *Wea. Forecasting*, **30**, 1819–1844, doi:10.1175/WAF-D-15-0068.1.

Storer, R. L., S. C. van den Heever, and G. L. Stephens, 2010: Modeling aerosol impacts on convective storms in different environments. *J. Atmos. Sci.*, **67**, 3904–3915, doi:10.1175/2010JAS3363.1.

Tao, W. K., X. Li, A. Khain, T. Matsui, S. Lang, and J. Simpson, 2007: Role of atmospheric aerosol concentration on deep convective precipitation: Cloud-resolving model simulations. *J. Geophys. Res. Atmos.*, **112**, D24S18, doi:10.1029/2007JD008728.

Tao, W. K., J. P. Chen, Z. Li, C. Wang, and C. Zhang, 2012: Impact of aerosols on convective clouds and precipitation. *Rev. Geophys.*, **50**, doi:10.1029/2011RG000369.

Thompson, R. L., 1998: Eta Model storm-relative winds associated with tornadic and nontornadic supercells. Wea. Forecasting, 13, 125–137

Thompson, R. L., and Coauthors, 2003: Close proximity soundings within supercell environments obtained from the Rapid Update Cycle. *Wea. Forecasting*, **18**, 1243–1261, doi:10.1175/1520-0434(2003)018<1243:CPSWSE>2.0.CO;2.

Thompson, R. L., C. M. Mead, and R. Edwards, 2007: Effective storm-relative helicity and bulk shear in supercell thunderstorm environments. *Wea. Forecasting*, **22**, 102–115, doi:10.1175/WAF969.1.

Twomey, S., and S. Twomey, 1977: The influence of pollution on the shortwave albedo of clouds. *J. Atmos. Sci.*, **34**, 1149–1152, doi:10.1175/1520-0469(1977)034<1149:TIOPOT>2.0.CO;2.

Van Den Broeke, M. S., 2013: Polarimetric radar observations of biological scatterers in hurricanes Irene (2011) and Sandy (2012). *J. Atmos. Ocean. Technol.*, **30**, 2754–2767, doi:10.1175/JTECH-D-13-00056.1.

Van Den Broeke, M. S., 2016: Polarimetric variability of classic supercell storms as a function of environment. *J. Appl. Meteor. Clim.*, **55**, 1907–1925, doi:10.1175/JAMC-D-15-0346.1.

Van Den Broeke, M. S., 2017: Polarimetric radar metrics related to tornado life cycles and intensity in supercell storms. *Mon. Wea. Rev.*, **145**, 3671–3686, doi:10.1175/MWR-D-16-0453.1.

Van Den Heever, S. C., and E. Al, 2006: Impacts of nucleating aerosol on Florida storms. Part I : Mesoscale simulations. *J. Atmos. Sci*, **63**, 1752–1775, doi:10.1175/JAS3713.1.

Van den Heever, S. C., G. L. Stephens, and N. B. Wood, 2011: Aerosol indirect effects on tropical convection characteristics under conditions of radiative–convective equilibrium. *J. Atmos. Sci.*, **68**, 699–718, doi:10.1175/2010JAS3603.1.

Weather Decision Training Division (WDTD), 2013: Dual-polarization radar training for NWS partners. Accessed 10 October 2018. [Available online at https://training.weather.gov/wdtd/courses/dualpol/Outreach/.]

Wakimoto, R. M., and V. N. Bringi, 1988: Dual-polarization observations of microbursts associated with intense convection: The 20 July storm during the MIST project. *Mon. Wea. Rev.*, **116**, 1521–1539, doi:10.1175/1520-0493(1988)116<1521:DPOOMA>2.0.CO;2.

Wang, C., 2005: A modeling study of the response of tropical deep convection to the increase of cloud condensation nuclei concentration: 1. Dynamics and microphysics. *J. Geophys. Res. Atmos.*, **110**, D21211, doi:10.1029/2004JD005720.

Wang J., S.C. van den Heever, and J.S. Reid, 2009: A conceptual model for the link between Central American biomass burning aerosols and severe weather over the south central United States. Environ. Res. Lett., 4, 015003, doi:10.1088/1748-9326/4/1/015003.

Wilson, J. W., C. A. Knight, S. A. Tessendorf, and C. Weeks, 2011: Polarimetric radar analysis of raindrop size variability in maritime and continental clouds. *J. Appl. Meteor. Clim.*, **50**, 1970–1980, doi:10.1175/2011JAMC2683.1.

Wolff, C. (n.d.). *Radar Basics*. Retrieved from radar range equation for weather radar: Accessed 16 October 2018.
[Available online at: http://www.radartutorial.eu/15.weather/wx05.en.html.]

Wurzler, S., T. G. Reisin, and Z. Levin, 2000: Modification of mineral dust particles by cloud processing and subsequent effects on drop size distributions. *J. Geophys. Res. Atmos.*, **105**, 4501–4512, doi:10.1029/1999JD900980.

Yuan, T., L. A. Remer, K. E. Pickering, and H. Yu, 2011: Observational evidence of aerosol enhancement of lightning activity and convective invigoration. *Geophys. Res. Lett.*, **38**, L04701, doi:10.1029/2010GL046052.

Zipser, E. J., D. J. Cecil, C. Liu, S. W. Nesbitt, and D. P. Yorty, 2006: Where are the most: Intense thunderstorms on Earth? *Bull. Amer. Meteor. Soc.*, **87**, 1057–1071, doi:10.1175/BAMS-87-8-1057.

Zrnić, D. S., V. M. Melnikov, and A. V. Ryzhkov, 2006: Correlation coefficients between horizontally and vertically polarized returns from ground clutter. *J. Atmos. Ocean. Technol.*, **23**, 381–394, doi:10.1175/JTECH1856.1.